12-2012

Double Paddle Oscillators for the Mechanical Spectroscopy of Ion-Solid Interactions

Jason Puls
Clemson University, jrpuls@gmail.com

Double Paddle Oscillators for the Mechanical Spectroscopy of Ion-Solid Interactions

---

A Thesis
Presented to
the Graduate School of
Clemson University

In Partial Fulfillment
of the Requirements for the Degree
Master of Science
Materials Science and Engineering

---

by
Jason R Puls
December 2012

Accepted by:
Dr. Chad E. Sosolik, Committee Chair
Dr. Marian S Kennedy
Dr. Fei Peng

To the greatest parents

Larry and Marry Ellen Puls

Acknowledgments

As I am starting to finish my thesis I have begun to reflect on all of the people that made this work possible. First off I would like to thank Dr. Chad Sosolik who was my advisor and committee chair. Without his guidance, none of this work would have been possible. If he had not kept me pointed in the right direction I would still be chasing around experiments and would never have finished any of them. Also, I would like to thank Dr. Sosolik and the Department of Physics and Astronomy for allowing a ”materials engineer" to teach physics classes as a teaching assistant. In addition I would like to thank Dr. Tom Metcalf who was one of the main reasons this whole project came together. I would like to thank him for the double paddle oscillators (DPOs) that he sent us. Without him this project would never have started because we do not posess the equipment to produce our own DPOs. Also, I would like to thank Tom for the invitation to visit his lab at the US Naval Reseach Laboratory and allowing me to see how a working DPO excitation system is supposed to function.

I would like to give a special thanks to Mr. Jon Simpson and Mr. Lamar Durham in the Physics and Astronomy instrumentation shop. Without these two amazing machinists/engineers this experiment would have taken many times longer. I would also like to thank them for putting up with all of my design mistakes and all of the rush jobs I dumped into their laps.

In the my laboratory I would like to thank Mr. Endu Srinadhu, Mr. Selcuk Temiz, Mr. Dhruva Kulkarni, Mr Radhey Shyam, and Mr. Daniel Field. They definitely made my life in the lab alot more enjoyable with enjoyable and challenging discussions. I would like to thank Daniel for helping me with my experiment design and for shooting down my ridiculous ideas thus keeping me realistic. Endu definitely made my life easier by helping me take some data so that I could focus on writing this thesis. Dhruva was a great resource for programming tips and for keeping my physics correct. All of my lab-mates pitched in from time to time when I needed an extra hand or got in over my head.

I would like to thank a large number of people in Clemson for keeping me sane, however the list would be too long to fit in this page. Most of those people I met at Backstreets Bar and Grill, which became my hangout and was a great place to play some pool and get away from the lab. American Pool Association (APA) leagues were a great outlet to focus on when I was out of the lab. All of my team members on the ”8-Body Problem" always encouraged me in my academic endeavors as most were graduate students as well.

I would like to thanks Mr. Jay Vaughn for allowing me to work at Systems South from a young age. The skills I learned while I was there are one of the biggest reasons that I made my way into experimental science. Without all of those afternoons and summers of work, I would never have learned many of the skills that I used to tackle my research. I would also like to thank Mr. Jim Lane who taught me the basics of machine design and how a strong baground in science can help you tremendously in engineering.

I would also like to thank my sister, Mrs. Emily George, for putting up with all my quirks and reminding me time and again of important dates and events that I probably would have completely missed. Finally, I would like to thank my

parents Dr. Larry and Mary Ellen Puls for their love and support throughout my time here in Clemson. Anytime I felt down or stressed, a phone call to either of them would always make me feel better. Their support has been invaluable to my entire academic career. The moral values and work ethic they both taught me have ensured that I always know where I am going, and how I am going to get there.

Table of Contents

List of Figures

Chapter 1

Introduction to Ion Bombardment

1.1 Ion - Solid Interactions

Ion-solid interactions can produce a wide range of changes to intrinsic material properties. Ion bombardment is widely used in semiconductor doping and tooling fabrication. Doping with ion beams is commonly called ion implantation. During implantation ions undergo both elastic and inelastic scattering leaving some of the ions inside the bulk. This causes some of the bulk atoms to be ejected but a number of them are merely displaced as the ions collide with bulk atoms through multiple atomic layers before coming to rest. This whole implantation cascade can thoroughly change the bulk properties near to the surface.

Implantation interactions are largely made of up two processes, nuclear and electronic stopping. Nuclear/electronic stopping relate scattering phenomenon between a crystal atom and the incident ion. Nuclear stopping is between the nucleii of the bulk atoms and the ion. Electronic stopping occurs after impact when the ion's electrons interact with electrons from bulk atoms, causing the ion to slow down. The electronic drag mostly contributes to heating of the surface. Stopping

of both kinds can lead to hole and path formation as the ion literally pushes itself into the bulk lattice as seen in Fig 1.1. As the ion penetrates it can displace atoms in the crystal. This displacement can cause an amorphization in the crystal structure, which is when the crystal lattice is broken down forming an amorphous layer. [1].

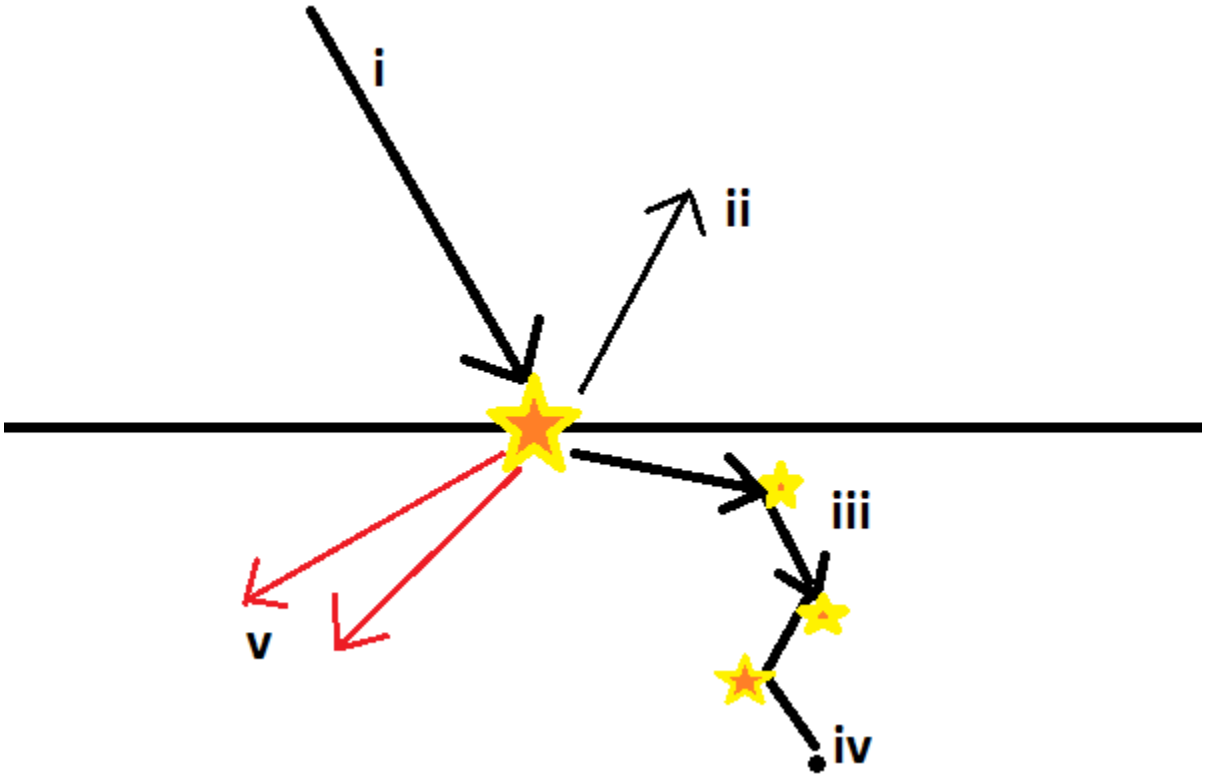

Figure 1.1: Drawing of an incoming ion impacting the surface and possible stopping processes: i. incoming ion, ii. ejected atom(s), iii. collisions, iv. implantation, v. heating

Major changes occur due to the ions ending up inside the substrate. Some of the implanted atoms end up inside the lattice as interstitials. These interstitials can produce a local stress concentration in the lattice as the ions, non-uniformly, change the lattice constant with respect to a pure crystal [2]. The strain produced

by this stress concentration can induce swelling at the implantation depth. If the dose is large enough, an additional phase may appear in the implanted region. These changes will lead to modifications in the overall bandgap of the sample in this region. Chemical modifications may also take place producing changes in the chemical potential as used in semiconductor doping.

Other major structural changes often occur in the crystal. As seen in past studies, ions tend to break up the crystal to the point it can become entirely amorphous in the regions above and inside where the ions came to rest [3]. This leads to a change in volume. The change in volume at the surface can incite curvature in the bulk if the sample is thin enough and it can cause a stress field to form near the amorphous crystal boundary if the sample is thicker [4]. This implanted ion stress can be used to make the surface of a material harder for tooling [5]. This new amorphous structure can cause large changes in the allowed states of the bulk leading to changes in optical and mechanical bandgaps. This is already used in industry for modifying optical sensors and photovoltaics [6]. However the long term stability may be changed because of the unstable nature of this new phase and its effect on the crystal phase beneath it.

After irradiation, relaxation can occur in the sample. Some of the lattice will recrystallize to minimize energy and diffusion of defects can occur. Diffusion of the ion species, the bulk matter, and defects at room temperature will generally take place over several hours unless the energy of the system is raised. Typically after ion implantation into semiconductor devices annealing is carried out to try to recrystalize the surface and freeze in the dopant atoms. This annealing is designed to increase the diffusion rate of the defects and the bulk such that they consume each other to reform the crystal. Without this increase in energy there is normally an increase in surface stress due to larger amorphous regions inside

the bulk and some of the foreign species will diffuse out through the damaged region and evaporate.

Current experiments for studying mechanical changes caused by ion irradiation are somewhat limited in their accuracy and few can be carried out in real time. Some studies have been performed using oscillating cantilevers but due to low quality factors their resonant frequencies have large bandwidths increasing their error. Sensing is also performed optically which can introduce noise [7]. In other cases cases a thin strip of material is irradiated in a vacuum chamber and a minute change in curvature can be measured optically [8, 9]. If the curvature is to be read in real time, the optical setups are often complicated because of their remoteness to the sample because most of the optical apparatus must be located outside of the vacuum chamber and must read the sample through windows. This technique only probes changes in the relative volume of the irradiated surface, leading to bending, which must be related to mechanical properties. Change in the shape may not directly correlate to a change in the modulii because heating, amorphization, and implantation depth all play a role in changing the curvature of the sample.

1.2 Oscillators

In many scientific fields, mechanical oscillators are used as senesors for measuring slight changes do to their resonant frequencies being highly dependant on their physical parameters. [10, 11, 12]. This is because the oscillator's resonance frequencies are dependent on the shear modulus, the moment of inertia, and the damping. By slightly altering these parameters, the resonance frequency can be altered as well. Piezoelectric oscillators, such as quartz, have become com-

monplance in most modern electronics for their frequency stability [13]. Quartz crystal microbalances (QCMs) use the surface wave effect to probe mass change on its surface and have the resolution to measure the formation of single atomic layers [14]. Certain oscillator designs have been used to measure small mechanical changes induced by low temperature noble gas sublimated and adsorbed on them. These devices are double paddle oscillators (DPOs) and have demonstrated precision to parts per billion when measuring shear modulii of these noble gas films. A typical DPO is shown in Fig. 1.2. This work was carried out by Tom Metcalf in the Department of Physics at Cornell University and later at the US Naval Research Laboratory [15]. Tom collaborated with my group and I by offering his expertise in DPOs. He also supplied the DPOs that were used in the experiments described in chapters 2 and 3.

Double paddle oscillators are a specially designed silicon oscillator that produces very large quality factors in certain resonance modes. The quality factor is defined as

$$Q \simeq \frac{\text{energy stored}}{\text{energy dissipated per cycle}} \tag{1.1}$$

Observing the frequency response of a real mechanical oscillator reveals a peak at expected resonance positions (in frequency) that have finite width. The width of the peak at full width half max (FWHM) divided by the resonant frequency is the inverse quality factor as seen in Fig. 1.3. The quality factor of a real mechanical oscillator is dependent on the resonant frequency and drag coefficient. The drag coefficient of an oscillator in a vacuum comes entirely from the internal friction of the oscillator. Because DPOs have a very high quality factor their peaks are very narrow, typically under 100 mHz. This reduces the noise in the resonant frequencies leading to more precise probing of their material properties. The

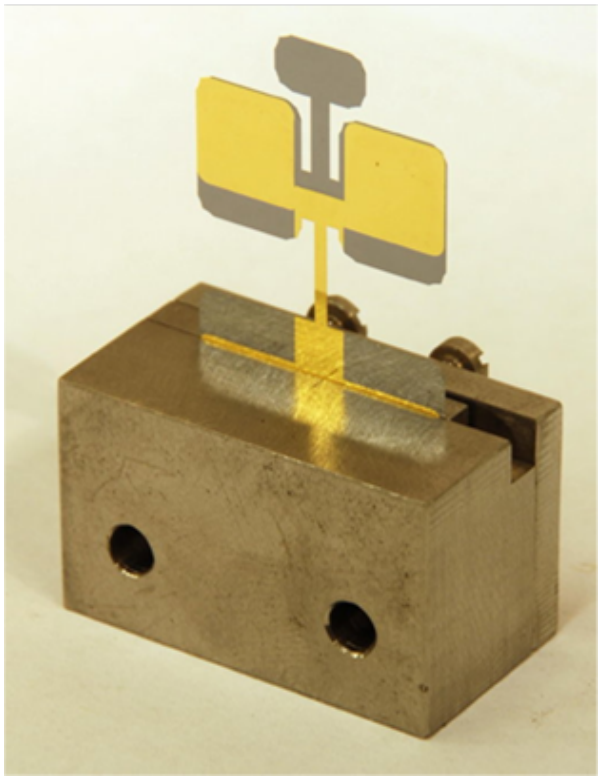

Figure 1.2: Back side of a DPO showing the gold contacts. The DPO is approximately 2 cm wide by 3 cm tall. It is around 300 μm thick. (Printed with permission from Tom Metcalf)

name ”double paddle" comes from the shape of the oscillator which resembles a large and small paddle connected via a small ”neck". This layout isolates the DPO from the clamping mechanisms because the two paddles oscillate with respect to each other not with the base. The shape of these oscillators was designed to focus all of the stress in certain resonance modes into the neck region between the two paddles and the head. Because of these design considerations, certain modes of the DPO have quality factors on the order of 10^6. This could be compared to the average acoustic tuning fork with a quality factor around 1000 [16].

This thesis will focus on irradiating DPOs for measuring mechanical changes in real time so that ion implantations and the resulting damage can be better un-

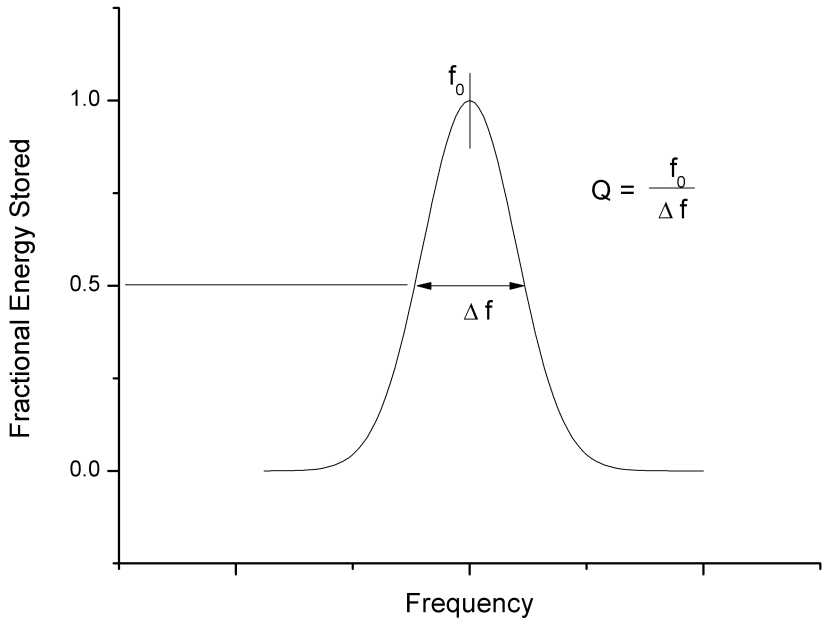

Figure 1.3: Determination of the quality factor in a damped driven harmonic oscillator. The resonant frequency divided by the full width at half maximum (FWHM) is the quality factor. DPOs resonanting in a certain mode in vacuum with a quality factor around 10^6 will have a width under 100 mHz.

derstood. Low energy ion implantation was used ($\leq 3keV$) for measuring the limits of the DPO as a sensor. In this energy regime the ions penetrate a small distance (<300 Å). In a SRIM simulation of 3 keV Ar ion implantation on Si, the implantation profile of Fig. 1.4 shows that the majority of the ions end up implanted near 100 Åbeneath the surface. This was the maximum energy used in this work and hence the maximum depth of implantion. This causes a film-like region with different mechanical properties to form. This region and its effect on the resonant frequency will be the focus of much of this work. The reason for this is that the change in resonant frequency is proportionall to the modification in the

"spring conastant" of the DPO which is related to the shear modulus. This is similar to modifying a simple damped driven harmonic oscillator. By utilizing certain resonance modes, changes in mass can be neglected because of the minute effect on the system. This is due to the moment of a torsional oscillator is porportional to the distance from the its axis.

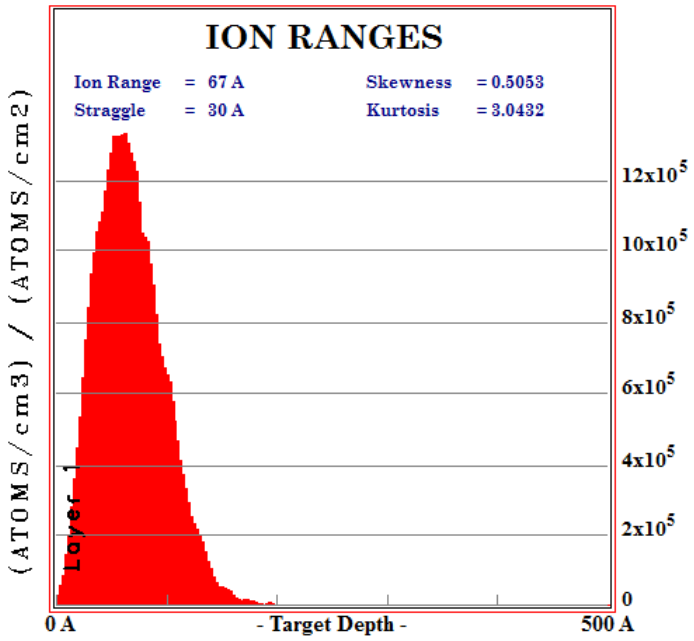

Figure 1.4: Implantaion depth profile from SRIM at 3keV for Ar in Si. At this incident energy most of the ions end up implanted beneath the surface.

Chapter 2

Excitation and Bombardment of DPOs

2.1 Overview of Experimental Setup

To properly measure shear modulus of a surface under ion bombardment with high precision a mechanical oscillator was used. As the principles behind oscillators are very well understood the DPO was applied for our experiment. The mechanical oscillator is a double paddle oscillator (DPO) that was originally used to measure low temperature thin films. We then repurposed this device for our work. A double paddle oscillator has a very large quality factor that is in the 10^6 range, where an average tuning fork only has a Q of approximately 1000.

The process of taking data requires a custom-built set of electronics and vacuum equipment that are used together to bombard and excite the DPO. Within the chamber the DPO is clamped on a manipulator that also holds a Faraday-cup, excitation electrodes, and a thermocouple. The vacuum chamber in which the DPO is placed is an OMICRON-STM analysis chamber, as seen in Fig 2.1. An

OMICRON-ISE10 ion gun was used to bombard the DPO with Ar^+ ions. The electronics were connected by feed-throughs to the electrodes mounted *in situ*. The custom electronics consist of an amplifier, a lock-in, a biasing box, a frequency counter, and a phase shifter. Most of the systems are monitored and controlled through IEEE-488 GPIB.

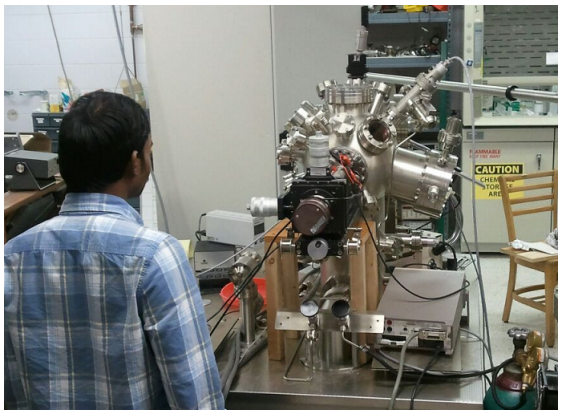

Figure 2.1: Image of UHV Bombardment Chamber located in Kinard Laboratory of Physics, Room 13. The Ion gun can be seen at a 45 degree angle on the right side of the chamber with a grey wire protruding from its end. The manipulator is the dark colored arm extending out from the sphere in the center of the image. One of my peers is in the foreground for scale.

In the following sections I will lay out the basics of the setup that we use to excite the DPO, bombard it, and measure the changes in the resonant frequency and quality factor. First, I will cover the DPO and the theory behind its excitation. Next, I will talk about the manipulator holding the DPO and its considerations. Then, I will explain the electronics behind taking data, and I will discuss how bombardment runs are performed, presenting some basic data that verifies that the system works as intended.

2.2 Double Paddle Oscillators

The double paddle oscillator is a device that is typically cut from a silicon wafer and is designed to have a very high quality factor in certain of its resonance modes. This device was invented at Bell Laboratories with the goal of finding devices with high quality factors [17]. It was also used at Cornell University to measure shear modulii of the DPO and thin films applied to it [18]. The DPOs I used were etched with KOH from a <100> silicon wafer, taking full advatage of anisotropic KOH etch rates in silicon. Tom Metcalf, who works out of the Naval Research Laboratory in Washington DC prepared the DPOs used here. Detailed steps concerning the fabrication of DPOs can be found in Ref. [18].

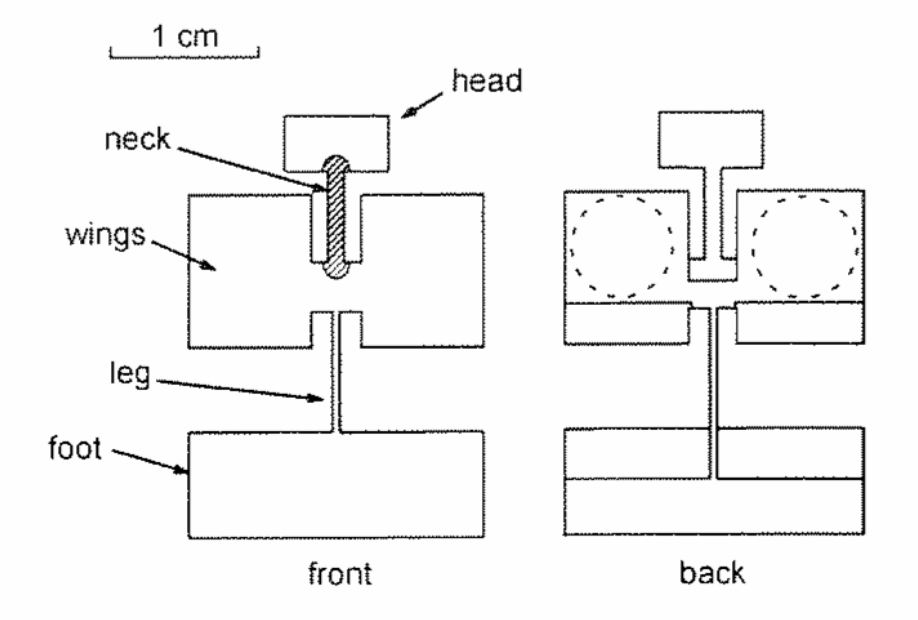

Figure 2.2: Diagram of simple double paddle oscillator with its parts labeled. The lines on the right side represent where the gold film is located. The dashed circles represent the electrode size with respect to the DPO. The actuall electrodes are positioned underneath the paddles slightly forward of this position towards the head.

The double paddle oscillator is approximately 2 cm by 3 cm. One side of the DPO is given a thin ($\sim 100nm$) gold coating to assist in electrode coupling. A DPO drawing with its parts labeled can be seen in Fig 2.2. The shaded region on and around the neck in Fig 2.2 is where the bombardment of Ar^+ takes place in this study. The second antisymetric mode (AS2) is the primary resonance mode that was used to take measurements and exists near 5.5kHz. An image of displacement in the AS2 mode from FEA analysis, using COMSOL, can be seen in Fig 2.3. FEA analysis of stress in a DPO resonating in the AS2 mode was also performed and is illustrated Fig 2.4. This shows that the energy stored during a cycle is concentrated in the neck, making small changes to the neck more easily observable. Also, much of the previous work concerning DPOs was focused on this mode, allowing us to compare our initial work with data already taken [18, 17, 15, 16, 19, 20]. The AS2 mode was used for our experiments and previous studies because the neck, where bombardment takes place, affects the resonance frequency by a negligible amount when it loses mass. This helps to reduce the effect of ion sputtering. The moment of inertia of the neck changes the resonance little, while the modulii of the neck has a much larger effect on the resonance of the system.

The AS2 mode of the DPO is excited electrostatically by a time dependant voltage. If an oscillating electric signal was used then the DPO would oscillate at twice the resonance frequency. To prevent this a DC bias is added. The bias also linearizes the signal. To see this we note that the force on the DPO is proportional to the square of the voltage applied to it:

$$F \propto V^2 \tag{2.1}$$

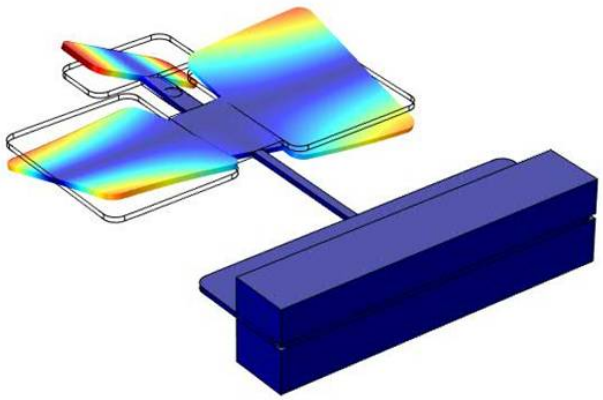

Figure 2.3: Displacement of a DPO resonanting in the AS2 mode as observed in a COMSOL finite element simulation.

If a sinusoidal signal is applied to the DPO,

$$V = V_{drive}\cos(t\omega) \tag{2.2}$$

then the force felt by the DPO is

$$F \propto V_{drive}^2(1 + \cos(2t\omega)). \tag{2.3}$$

This means that the DPO will actually be driven at the second harmonic of the driving signal. This result would require a much more complicated system to self resonate. To fix this the signal is biased with a DC voltage much larger than the driving voltage

$$V_{bias} \gg V_{drive}. \tag{2.4}$$

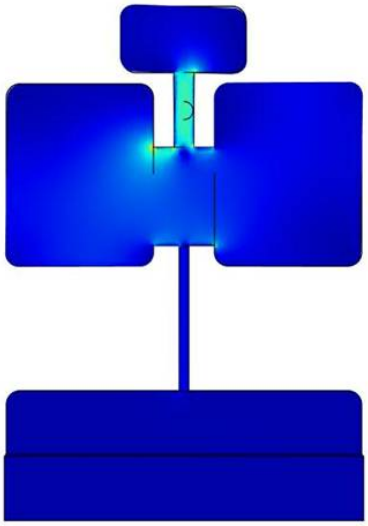

Figure 2.4: Maximum stress in a DPO modeled using COMSOL. This shows that the majority of the energy stored during oscillations in the AS2 mode, is stored in the neck of the DPO.

This modifies the force in equation 2.3 into

$$F \propto (V_{bias} + V_{drive}\cos(\omega t))^2 \tag{2.5}$$

which can be approximated to

$$Force = V_{bias}^2 + V_{bias}V_{drive}cos(\omega t) \tag{2.6}$$

by dropping the smaller second harmonic term $cos(2t\omega)$. This both improves the effect of the driving signal on the DPO and linearizes the signal. The actual device used to carry this out is the "battery box" and will be explained in the next section [15].

In the second antisymetric mode, the DPO is basically a torsional harmonic oscillator. Similar to a simple theoretical harmonic torsional oscillator, factors that

control the resonance frequency are the "spring constant" and the moment of inertia. This "spring constant" is dependent on the modulii which is also dependent on the temperature. To determine the effect of ion bombardment on the modulii of the DPO we try to hold the temperature constant and observe the change in resonance frequency to determine how much we have affected the material. The resonance frequency is proportional to the shear modulus (G) and the shape (j).

$$f_r \propto jG/4\pi \tag{2.7}$$

. Because the DPO is dependent on G, this was how I determined the effect of the ion bombardment on actual material changes [21]. The actual "spring" of the DPO is a sum of all the modulii throughout the entire neck. Because the neck is around 300 um thick and we are only bombarding the first few monolayers of silicon, 10-20 nm, then the small changes in the resonance demonstrate the precision of this instrument.

There are several additional modes under 10 kHz that can be excited with this method. We were able to "ring up" most of the modes as seen in Fig. 2.5 by scanning from 1 to 9 kHz except for the windshield wiper modes where the DPO oscillations are perpendicular to the driving forces. With alternative electrodes all modes might have be able to be seen; however, since we were focusing on only the AS2 mode this was not our goal [**?**].

2.3 Electronics

For the shear modulii to be measured in real time, the DPO is driven in a self resonating loop while it is bombarded with ions. The core of the system is

Mode name	Abbreviation	Symmetry	Eigenfrequency calculated f_{calc} (Hz)	Eigenfrequencies measured f_1 (Hz)	f_2 (Hz)	f_3 (Hz)	f_4 (Hz)
1st cantilever	CL1	+	280	250	253	251	245
symmetric torsion	ST	−	441	419	409	418	410
1st windshield wiper	WW1	n/a	889				738
2nd cantilever	CL2	+	1703	1634	1577	1612	1602
3rd cantilever	CL3	+	3340	3134	3174	3106	3068
1st antisymm. tor.	AS1	−	4728	4911	5323	4890	4791
1st flapping	FL1	+	5294				5184
2nd antisymm. tor.	AS2	−	5515	5561	5902	5483	5307
2nd windshield wiper	WW2	n/a	6254	⋆	6941	6487	⋆
3rd windshield wiper	WW3	n/a	12 189	⋆	⋆	⋆	⋆

Figure 2.5: The predicted and measured frequencies of the first 10 modes of a DPO as seen in previous work [16].

a SRS-830 lock-in amplifier and a custom phase shifter. The DPO's frequency is monitored by a frequency counter, SRS-620, and the temperature is monitored by an electrometer. The quality factor of the DPO can be measured by turning off the driving frequency and measuring the ring down with the lock-in.

As seen in Fig 2.6 the first connection to the DPO is the "battery box". The "battery box" we built does not actually have batteries in it, like the one built by Tom Metcalf, but is powered from a DC supply. The schematic of the "battery box" is seen in Fig2.7. The coupling capacitors are 0.1 uF and the large resistors are to prevent deadly discharges if a short occurs. The coupling of the electrodes to the DPO is on the order of pF. The equalization in the DC coupling capacitors that occurs when the power supply is turned on is well less than a second even with the large resistors. The resistors have also prevented the author

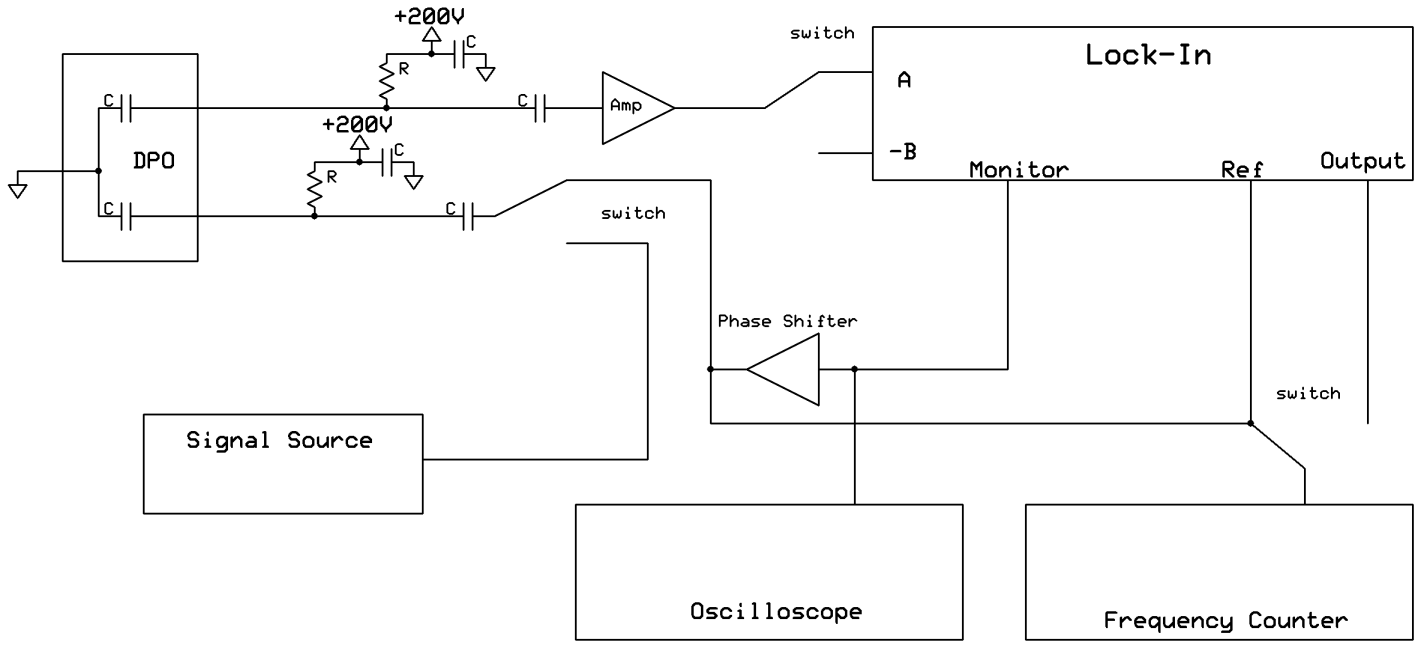

Figure 2.6: Entire DPO excitation electronics layout. The square labeled DPO shows electrical equivalent circuit of a DPO. The top line to the DPO is the return signal while the bottom line is the driving signal.

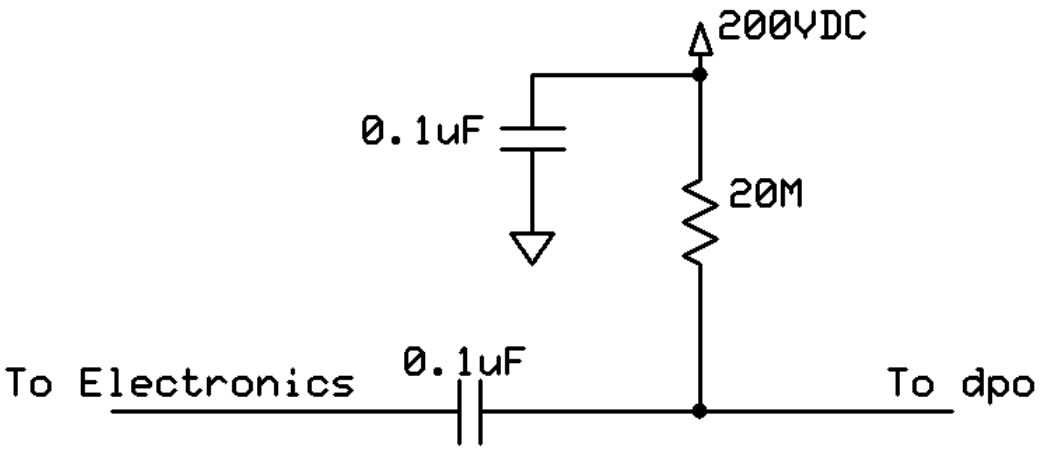

Figure 2.7: Schematic of the battery box internals. One circuits is used to decouple the bias voltage on both of the lines to the electrodes as seen in Fig. 2.6.

from electrocuting himself countless times as well. The other 0.1uF capacitors, connecting the DC input to ground, reduce outside electrical noise from reaching the DPO or its associated electronics. The DPO is driven at resonance, in short, by its own signal. Basically, the return from the "battery box" is amplified, phase shifted, and fed back into the DPO. This makes the DPO self resonating and it has been observed to hold its resonance frequency to around 0.003 Hz. The DPO is mounted inside of the vacuum chamber and connected to the electronics by feed-throughs. The signal is first fed into a custom built current to voltage converter (see Appendix B). It amplifies the signal close to $10^9 V/A$ before being fed into the lock-in amplifier. The current to voltage converter was custom built to operate between $\pm$12 V from an ATX power supply. Originally the lock-in was used for

amplification of the signal. However as its amplification was only 10^8 V/A the signal was very faint. During a disconnect, however, the amplifier was destroyed and a new one had to be constructed. With the new current to voltage converter a fully excited DPO will produce almost a $\pm$170 mV signal as seen at its output.

A lock-in, Stanford Research Systems SRS-830, is used to determine the amplitude for the ring down and can be seen, along with all the other electronics in Fig. 2.6. The reserve is set to low noise and the time constant to around 3μs. It is set to run in R θ mode to convert the oscillations into phase space. This just converts the real and imaginary parts of the signal to an amplitude and phase. The phase is with respect to the reference and has no real use in the majority of the data. The R output can be seen as the amplitude of the return signal and being relative has no real units. Determination of the actual displacement of the DPO was not done as the error in the measurements would have been large. To find the actual displacment, highly accurate measurments of the electrode dimensions and their separation would be required. Also the exact frequency response of the current to voltage converter would be required as well as its exact amplification. The displacment of the DPO could be determined by observing the actual voltage change with these variables known. These measurements would have been beyond the scope of this thesis and was not needed for ion irradiation measurements.

A signal is then fed from the Signal monitor side of the SRS-830 to the oscilloscope to observe it. Technically the lock-in is not needed for normal resonation of the DPO but it is generally always in the loop for ease of use when switching from resonance to quality factor measurements. Also the line filter on the lock-in helps reduce low frequency signals from appearing. Because the amplitude of CL1 and ST are very large the signal has a tendency to try to push into those

low modes during the self resonating loop. The line filters on the lock in tend to prevent the DPO from switching modes during long periods of resonation. The internal oscillator on the lock-in uses the return from the DPO to follow. When performing quality factor runs, as the signal drops in amplitude, the internal oscillator has a tendency to lose the signal and jump to high frequencies. To counteract this, the internal oscillator on the lock-in is manually tuned to $\pm$ 1Hz of the resonance to properly determine the amplitude. As long as the internal oscillator is set to around $\pm$1-5Hz of the actual frequency the measured amplitude is fairly close to the actual amplitude. This is mostly because the lock-in is set to R theta mode and not measuring the real and imaginary components.

The signal is split as it leaves the SRS-830. One of these goes to the oscilloscope to observing ringing and the other is fed into the phase shifter. The phase shifter, as we call it, is actually an all-pass filter built using a operational-amplifier [22]. The circuit is discussed more in Appendix B. The phase shifter has its frequency limits set to 1kHz to 10Khz and all signals in the range can be shifted by $\pm$ 90 degrees at varying resolution. If the signal needs to be set beyond this, the input of the lock-in can be changed to -B thus shifting the signal 180 degrees allowing any phase angle to be in range. By adjusting the gain of the phase shifter the output is always near $\pm$12V. All of this equipment is used to record the data for analysis. The procedure for carrying out the experiment is described below. The lock-in amplifier can be used to find the resonances of a new DPO and can determine the quality factor. To measure the frequency the DPO during bombardment a SR620 frequency counter is used. To measure the thermocouple a electrometer is used. All of these modules are controlled over a GPIB connection. Several programs written in Pascal perform these measurments. These programs can be seen in Appendix B.

2.4 Manipulator

The manipulator was re-designed for the purpose of holding the DPO securely, bombarding it with controlled ions, and monitoring it while resonating. The manipulator arm that was used came off of the original OMICRON chamber. The OMICRON platen holder that was originally on the arm was removed from the end. A new mount that fit on the end on the arm was designed to hold the bombardment side of the DPO in the center of its axis of rotation as seen if Fig. 2.8 The DPO itself was originally clamped by set screws but it was easy to over-stress a DPO breaking them. The clamp was re-designed to use a plunger set-screw that allows us to clamp via the screw's internal spring. This also holds the DPO firmly yet allows for easy loading and removal. A stainless steel mask is placed over the DPO with a small hole positioned over the neck. This mask prevents ions from implanting in any area other than the neck. Mounted 0.25 inches from DPO on the base is a thermocouple that monitors the temperature. While it may be separated from the DPO it gives an indication of the temperature of the DPO. In the future it will be used to calibrate the DPO's resonant frequency as a function of temperature.

As described in the previous section the DPO is excited using electrostatic forces. This is done using two electrodes that are made of copper as seen in Fig. 2.8. Each electrode is positioned to line up with the paddles. The electrodes are epoxied inside of copper tubes making them coaxial electrodes. As crosstalk became a large factor in the analysis of the data, shielding the electrodes in this manner was a step taken to reduce it. The electrodes also are held in place on the holder by set screws allowing them to be adjusted along their axis for varying separation from the DPO. Beyond 2-3 mm they will no longer excite the DPO in

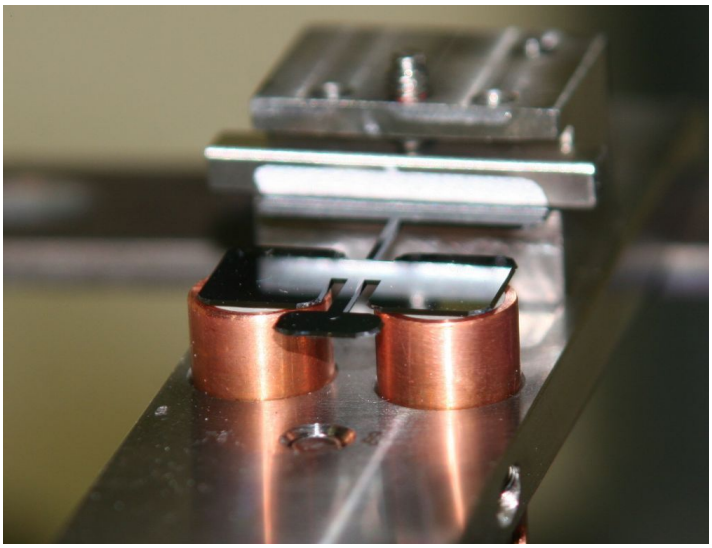

Figure 2.8: DPO holder and electrodes. This is an early picture of the manipulator head and does not include the mask or the thermocouple

any measurable amount, thus must be kept quite close (generally around 0.5-1 mm). Ideas for the improvement of the electrodes will be discussed in Section 4.4, Future Work.

The back side of the DPO manipulator has a Faraday Cup mounted on it. The cup is used to facilitate beam tuning. Because of its small opening, 0.4 mm, the spatial resolution of the beam can be measured. This information is then used to find the proper placement of the DPO and mask for accurate bombardment. The cup is made of copper and has a front collamination plate on it for improved spatial resolution. The front plate is grounded to prevent charge build-up and a Keithely electrometer is used to measure the current. The typical current is under 1-2 μA. The top plate is insulated from the cup by ceramic washers and the ground wire to the top plate is clamped under one of them. A closeup of the current manipulator head can be seen in Fig. 2.9 showing the electrodes, the DPO clamp, and the Faraday cup.

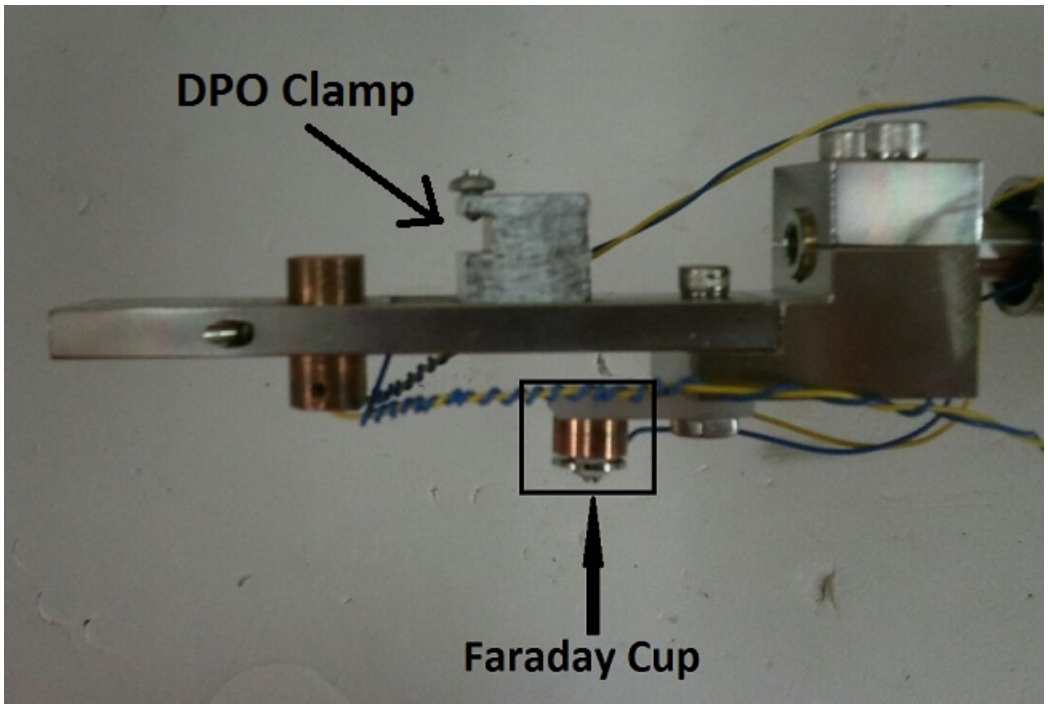

Figure 2.9: Side view of manipulator showing the Faraday cup and the DPO clamp.

2.5 Experimental Procedure

The experimental procedure can be broken into three parts. The first is the initial determination of the resonance frequency and ringing up of the DPO to the desired mode. The next is tuning up a beam and recording data during a bombardment run. The final procedure is measuring the quality factor. These different experiments are described below.

To get an enlarged signal and driving force as described in the previous section a floating 200VDC bias is used. The driving signal can be from either the frequency generator (SR650) or the phase shifter. As seen in Fig 2.6 the frequency generator (Standford Research Systems DS335) is used to initially ring up the DPO. Because the resonances vary between DPOs new ones must be scanned

with the *DPO.data* program. This can be performed by hand but can sometimes be very time consuming. This program scans the frequency generator between two frequencies at variable step size and records the R from the lock-in amplifier. After a scan, the resonances become very clear as seen in Fig. 2.10 where a range of 1-9 kHz was scanned. The signals appear non-Lorentzian because of the coupling. As higher vacuum is reached the peaks can become very narrow and make scanning very slow due to the necessarily smaller step size. To facilitate this process gas can be introduced through the ion gun to widen the peaks by increasing the drag. Two high resolution scans of the AS2 mode taken at $10^{-2} Torr$ are shown Fig. 2.11. The gas induced drag reduces the quality factor of the DPO, significantly widening the peak.

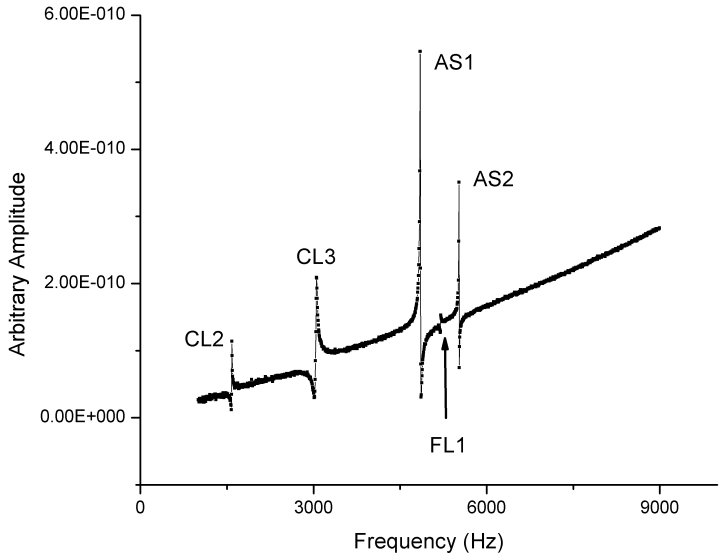

Figure 2.10: An example of a set of data from a new DPO scaned from 1-9 kHz indicating the resonance peaks.

Once resonance locations have been observed the frequency is tuned very

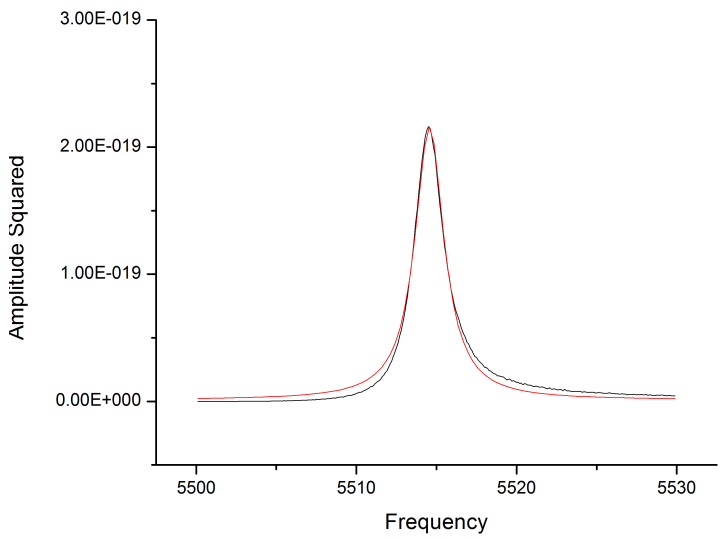

Figure 2.11: A pressure induced widening of the frequency response of a AS2 resonance mode. Two Scans are superimposed both taken at around $10^{-2} torr$.

close to the desired resonance using the frequency counter and the oscilloscope by hand. When an amplitude maximum has been achieved, indicating the DPO is sitting close to its resonance frequency, the phase shifter is fed into the oscilloscope. The frequency generator output is also split and observed simultaneously in the oscilloscope. The phase shifter is then adjusted to match the phase of the generator. The oscilloscope must have its trigger set to the frequency generator input throughout or the signal will be phase shifted by it. Once proper alignment is achieved, the input is switched over to the phase shifter and the DPO will ring up in amplitude. The signal monitor of the lock-in is also sent over to the frequency counter. When the DPO is resonating properly the frequency counter indicates high short term frequency stability (for several hours; some thermal drift occurs over a whole day).

Once the DPO is in the proper mode and the system is prepared for data

recording, the DPO's manipulator is rotated to point the Faraday cup at the ion gun, also shielding the DPO from stray ions. The OMICRON-ISE10 is tuned up and gas is introduced into the system. Once the gun is brought up to the desired energy and pressure then the manipulator and lenses can be adjusted to achieve maximum current. The manipulator has been used to measure the beam profile. A tuned beam has been measured to be around 1cm in diameter which is large enough to cover the whole neck through the mask. Then the gas can be adjusted to achieve proper beam current. Next the gun's accelerating voltage is switched off and the manipulator is adjusted, placing the DPO in position to be irradiated. The frequency counter is then read by GPIB at 1Hz intervals using the program *DPO.freq* for data measurements during bombardment and relaxation. Normally the program is left running for a few minutes before the bombardment to show the frequency is stable. After bombardment *DPO.freq* was often run for days as relaxation can take 20+ hours. The accelerating voltage can then be switched on and off as the particular experiment proceeds.

To measure the quality factor of the DPO the lock-in is used. A program, *DPO.Q*, measures the relative amplitude on the lock-in at 1 Hz intervals. The amplitude in this case is R from the R theta mode. The DPO must be first rung up by the method just described. Once the whole setup is ready and the program is running the signal going to the DPO is turned off. Initially the signal will suddenly drop as the coupling disappears. Then the amplitude will drop off in an exponential manner. If the natural log of the amplitude is calculated, the signal can be fit by linear regression to find the quality factor using the transient part of the following equation of a damped harmonic oscillator $f(t) = e^{-\lambda * t}\cos(\omega t)$. Our quality factor exhibited noise on the same order as the signal. Therefore data taken from it will not be considered until the precision can be improved.

During very long frequency scans some oscillations appeared. The oscillations had a period of between 10-12 hours. The thermocouple confirmed that heat flowing through the manipulator from the room was slightly affecting the frequency. FEA analysis was performed on the DPO and shows that thermal equilibrium between the manipulator and the DPO took place in just a few minutes. Some heating also occurs in the DPO's neck during bombardment and will be addressed further in the next chapter.

Chapter 3

Results

3.1 Introduction

DPOs were irradiated with Ar^+ ions inside an OMICRON-STM chamber and their resonant frequencies were recorded before, during, and after bombardment. When the DPO is under irradiation, the frequency of the resonant mode changes. This change may be related back to physical changes occuring inside the DPO's neck. Because we were unsure what we would see, we began at low energies and currents. Below 1 keV no effect was observed above the noise. However, this may have been caused by the low fluences produced by the ion gun at these energies($\leq 10^{14} ions/cm^2$). Because of this lack of observable change, all of the data from the energies below 1 keV were not considered in any analysis. The rest of the data consists of nine runs on two DPOs and is used as the basis for the majority of the following conclusions. Above 1 keV all the DPO resonance frequency plots took on a specific shape when graphed with respect to time. An example of this shape taken from one of the runs can be seen in Fig. 3.1.

We decided to divide the graph of the resonant frequency of the DPO

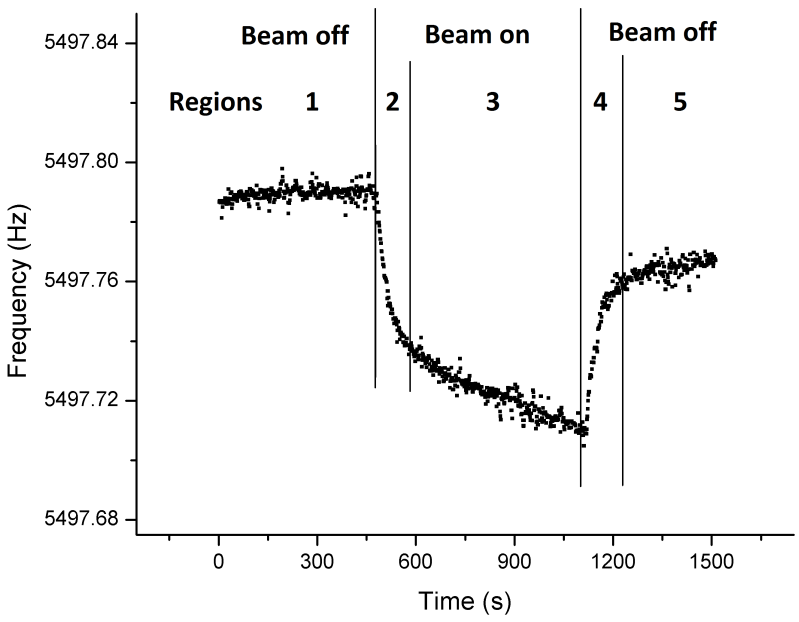

Figure 3.1: Five regions of interest in a data set showing the resonant frequency throughout a bombardment run.

during bombardment into several regions. The first region is simply the DPO resonating with no influence and is used for a reference. The second and fourth regions depicted on Fig. 3.1 can be related to a compressive stress caused by incident ions implanting into the crystal (Sec 3.2). The third region exists after region two goes linear and may be related to heating of the neck (Sec 3.3). The final region, region five, is after the beam has been turned off and region four has saturated. The resonant frequency in this final region relaxes over many hours eventually approaching the initial frequency. This reversable relaxation may be caused by heat or material diffusion (Sec 3.4).

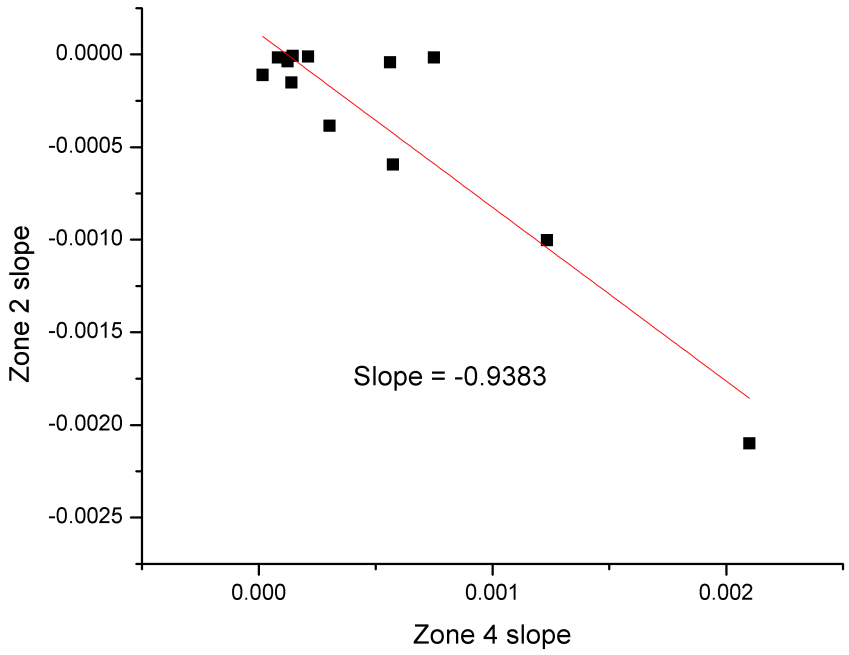

Figure 3.2: Comparison of the slopes of regions two and four of beam runs. The line is a linear fit of the data; the slope of this line is shown.

3.2 Compressive Stress

As ions bombard the DPO there is a compressive stress applied locally to implanted region inside the DPO neck. A slight pressure is applied to the neck of the DPO. I have estimated this to around μN, based on the ion beam fluence and energies. The torque on the leg can be ignored in our case because of our choice of modes. The second antisymetric mode relies on all energy being stored in the neck, separated from the leg by the paddles. Looking at the data we see that it takes around 20-40 seconds for the ions to saturate the implanted region. This saturation has been observed in other work using different ion species and substrate [1]. The incident ions can cause a swelling of the surface as they are

implanted into the substrate. This results in a reduction in the shear modulus because of swelling in the implanted zone. The resonant frequency of the an oscillator ,taken from the the equation of motion,

$$f \propto \sqrt{K/I} \tag{3.1}$$

where K is directly related to the modulii of the system and I is the moment. Loosening of the implanted zone in the lattice caused by the impacting atoms should reduce the frequency because it reduces k. Regions two and four of the bombardment runs were analyzed by taking the first 20 seconds of the drop before the DPO saturates. A comparison of the slopes of regions two and four is seen in Fig. 3.2. A linear fit applied to this data gives a magnitude of nearly one. This verifies regions two and four are not a heating event as the rates of heating and cooling would be drastically different because the sample is in vacuum. If regions 2 and 4 were caused by heating then we would see a slow rise in frequency when the beam was turned off instead of the sharp rise that we do see [8, 23].

The magnitude of the downward offset in the frequency caused by the beam should have a relationship with both beam energy and current. All of the runs were conducted over 1keV, well above the minimum implantation energy. We used SRIM to approximate this minimum energy, and found it to be around 300 eV. Because all of the ions are implanted into the bulk the energy should have to effect on the magnitude of the offset. The beam flux however is tied to the offset as seen in Fig. 3.3. A linear fit produces a slope of $2x10^{-14} Hz/ion/cm^2/s$ which seems small until one thinks in terms of $10^{15} ions/cm^2/s$, a typical fluence. This offset was taken by comparing the height of the end of region one with the end of region two. I defined the end of region two and the start of region three as the

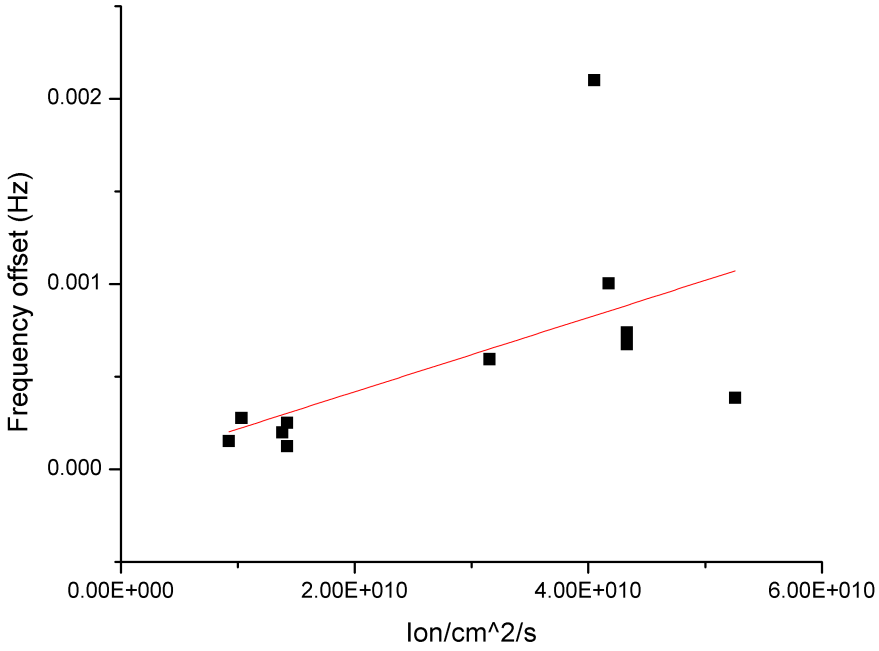

Figure 3.3: Offset caused by compressive forces

point where both regions change from nonlinear to linear, as indicated by the fits in Fig. 3.4. This method could be used to find the flux of an incoming beam with relative independence to the implantation energy. Small mechanical oscillators could be placed inside a ion implantation system and be used to find the number total implanted ions similar to how a QCM determines deposited film thickness.

3.3 Heating

In almost all bombardment runs there is a linear section during the actual ion bombardment as seen in Fig. 3.5. We believe that the linear frequency drop is caused by ion bombardment induced heating. This frequency change always a

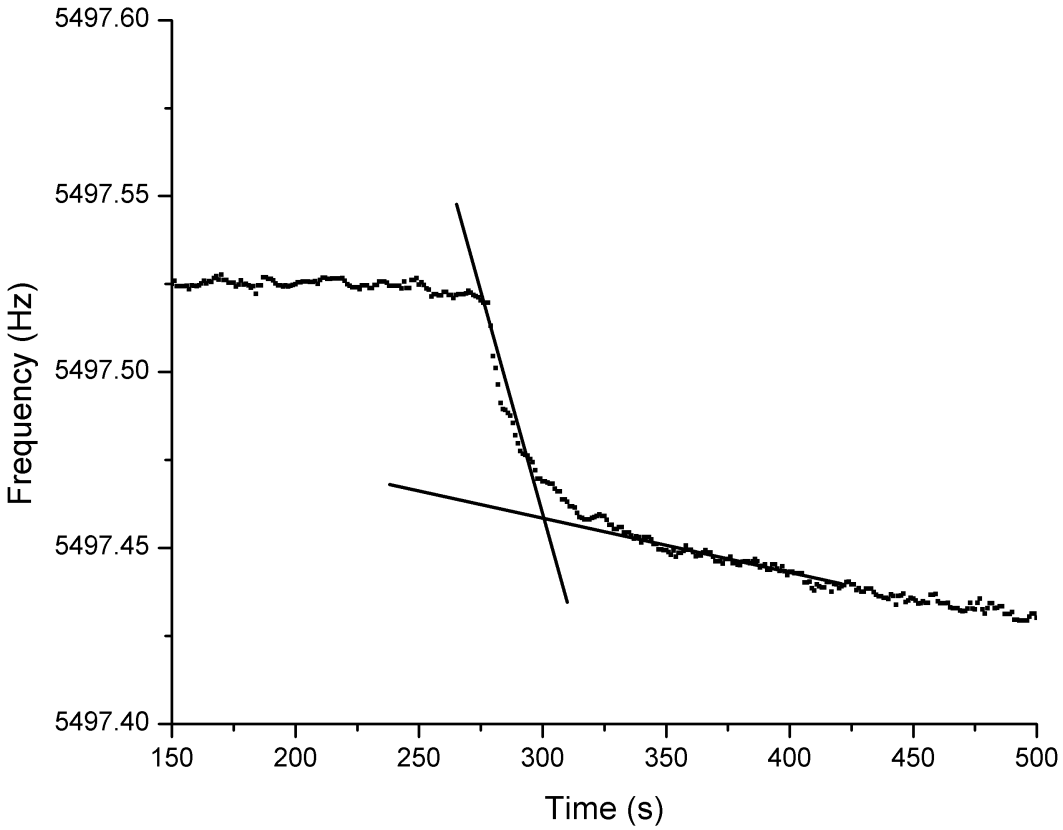

Figure 3.4: Change from region two to region three with the linear fits shown.

trend downward and we belive be tied to the relationship between the shear modulus and temperature. Young's modulus (E) is converted to the shear modulus (G) modulus with a material constant, Poisson's ratio, v.

$$G = \frac{E}{2(1+v)} \tag{3.2}$$

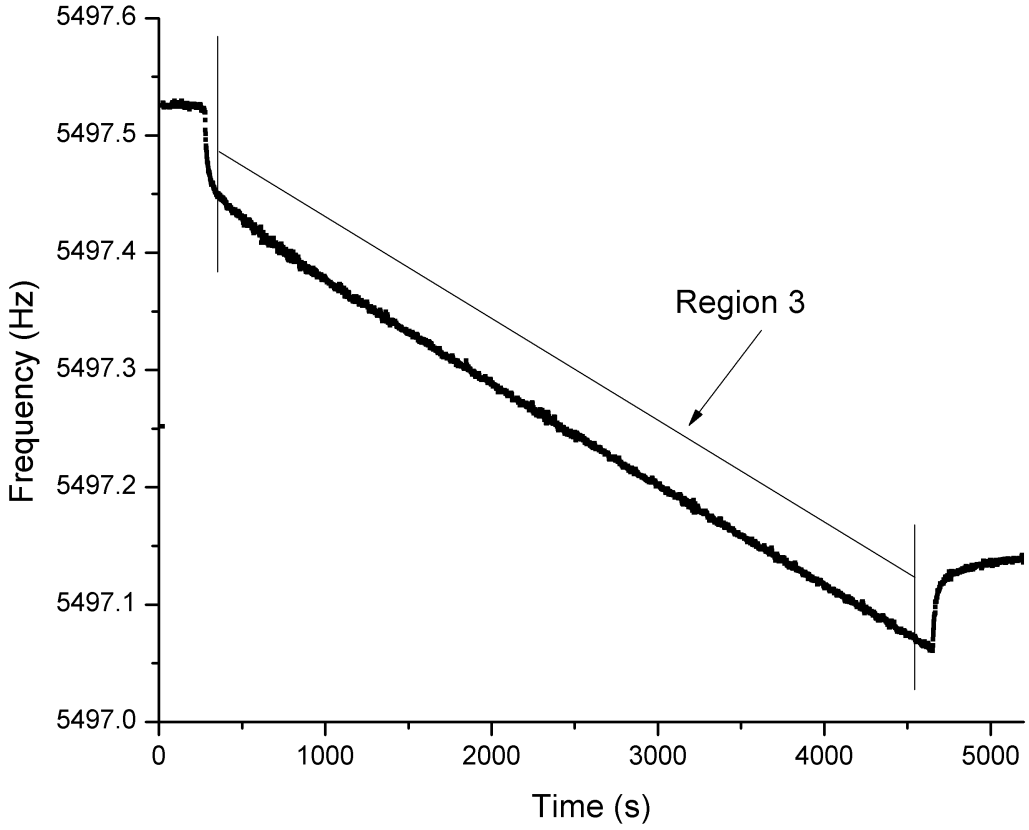

Figure 3.5: An example of a 3keV ion bombardment run. We think the heating is the linear region first 55 minutes.

. To explain the relationship between shear modulus and temperature we use the following equation.

$$E(T) = E_0 - BTe^{(T_0/T)} \tag{3.3}$$

E_0 is the initial Young's modulus. B and T_0 are material constants that define a relationship between youngs modulus and temperature in silicon. For silicon, B is equal to 0.158 1/K and T_0 is equal to 317 K [21]. Equation 3.3 can be expanded

into the following equation.

$$E(T) = E_0 - B + \frac{BT_0}{T} \tag{3.4}$$

This equation shows that a linear increase in temperature reduces Young's modulus as T_0/T. This function can be approximated as linear when T is less than T_0 as was the case for our expermient. To observe how the frequency changes in an oscillator undergoing a temperature change, we need to know how Young's modulus effects the frequency of an oscillator. The frequency of a torsional damped driven harmonic oscillator, which we think is a good simplification of a DPO oscillating in the AS2 mode, can be expressed as an equation that shows frequency is proportional to the spring constant, k and the moment, I.

$$f_r = \frac{1}{2\pi}\sqrt{\frac{k}{I}} \tag{3.5}$$

An expansion of this equation shows us that frequency changes linearly with k.

$$f_r = \frac{1}{4\pi}\frac{k}{I}. \tag{3.6}$$

As the ”spring constant" k is reduced, so is the frequency linearly reduced. The "spring constant”, k, is related to the shear modulus, G, by the following equation,

$$k = \frac{jG}{L} \tag{3.7}$$

where j is based on the shape/cross-section of the torsional spring and L is its length [24]. Combining equations 3.4, 3.6, and 3.7 gives an approximation of how

temperature changes the resonant frequency of the DPO.

$$f_r = C_1 + C_2 \frac{T_0}{T} \tag{3.8}$$

C_1 and C_2 are new constants produced through the combination of constants in equations 3.4, 3.6, and 3.7. Looking at a first order approximation of equation 3.8 it is evident that if the temperature of the oscillator linearly increases by small ammounts and remains less than T_0 the frequency will drop linearly [25, 26].

The temperature increase due to ion heating of the DPO neck can also be seen to be linear if the ion beam is constant, based on the definition of specific heat.

$$C = \frac{Q}{m\Delta T} \tag{3.9}$$

In this equation C is the heat capacity, m is the mass, $\Delta\ T|$ is the change in temperature, and Q is the heat. Assuming the ion beam is constant, the heat flow is directly related to the ion flux, then the temperature will increase linearly. Using the same method described in the previous section to define where section 2 began and ended, we found where section 3 began and ended and then dropped 15% of the data on either end to reduce error. Then linear regression was used to find the rate of change of resonant frequency for the AS2 mode. Using this data to find frequency change as a function of beam current led to the plot on Fig. 3.6. To find actual heat transfered one could simply convert the beam's kinetic energy (in eV) to joules; however to do this a measure of loss would need to me known. This loss would be tied to backscattered ions, sputtered atoms, or electromagnetic radiation. As the loss methods were unclear and were never measured the flux of the beam is expressed as current. SRIM can give an estimate of how much

this loss is. In a SRIM simulation of a 3 keV ion beam, 2.5 keV per ion was deposited into the substrate as heat. More SRIM runs at other energies predict that 85±2% of the energy per ion is deposited into the substrate through our entire energy range. Negating any heat loss other than conduction, a simulation using COMSOL was performed on a DPO under virtual bombardment using the energy loss ratio SRIM predicted. This simulation produced a plot showing the temperature in the neck of DPO under bombardment seen in Fig. 3.7.

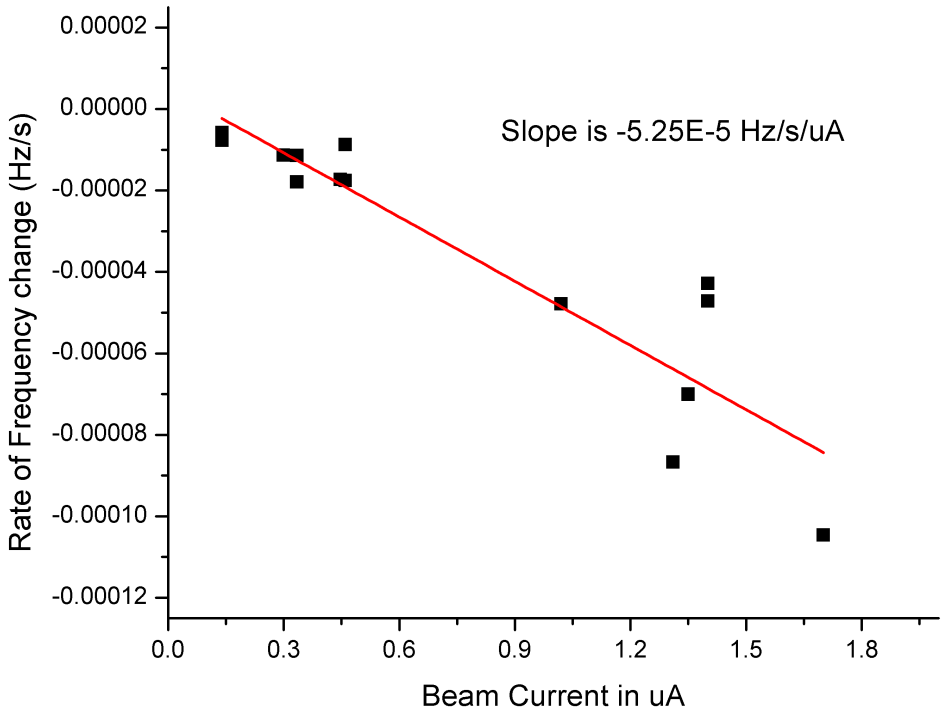

Figure 3.6: Beam current and its effect on the rate of frequency change. The line represents a linear fit of the data with the slope shown.

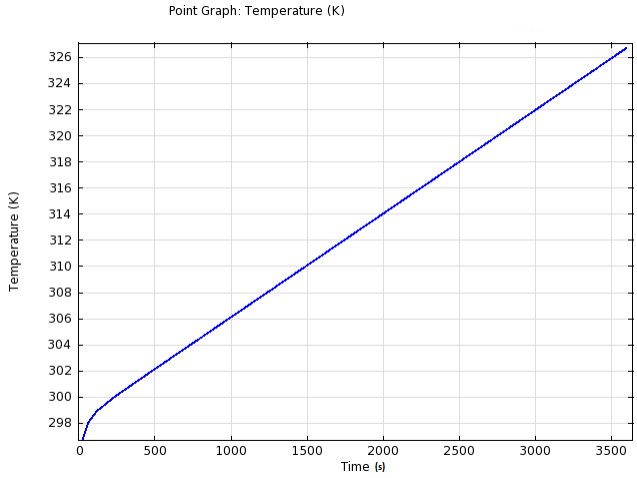

Figure 3.7: FEA analysis using COMSOL of heating of the neck under a 3 keV beam at $10^{+15} ions/cm^2/s$.

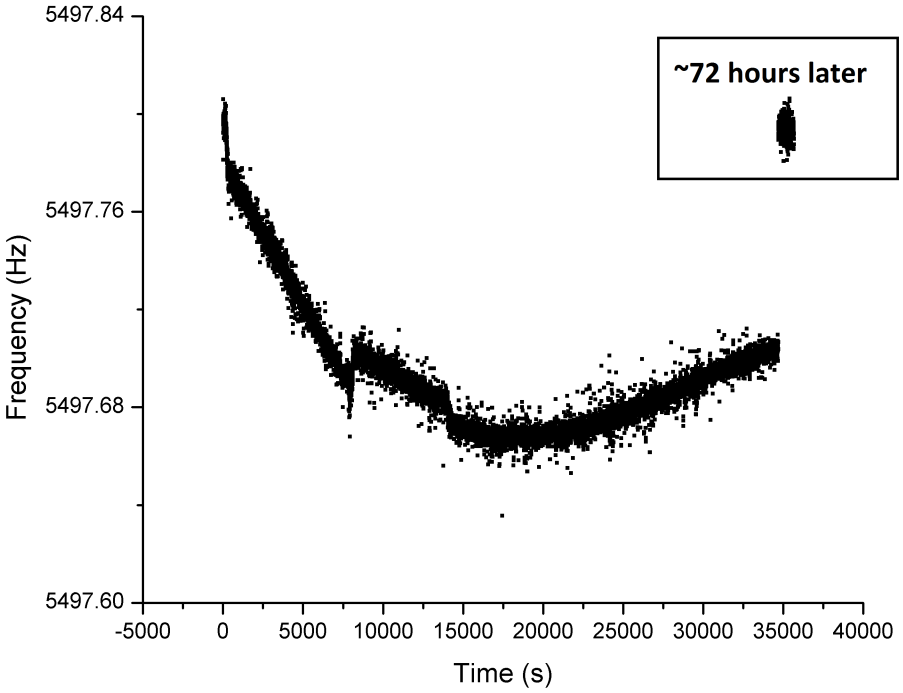

Figure 3.8: Bombardment run showing post bombardment relaxation. Inset box is a short run taken 72 hours after run began.

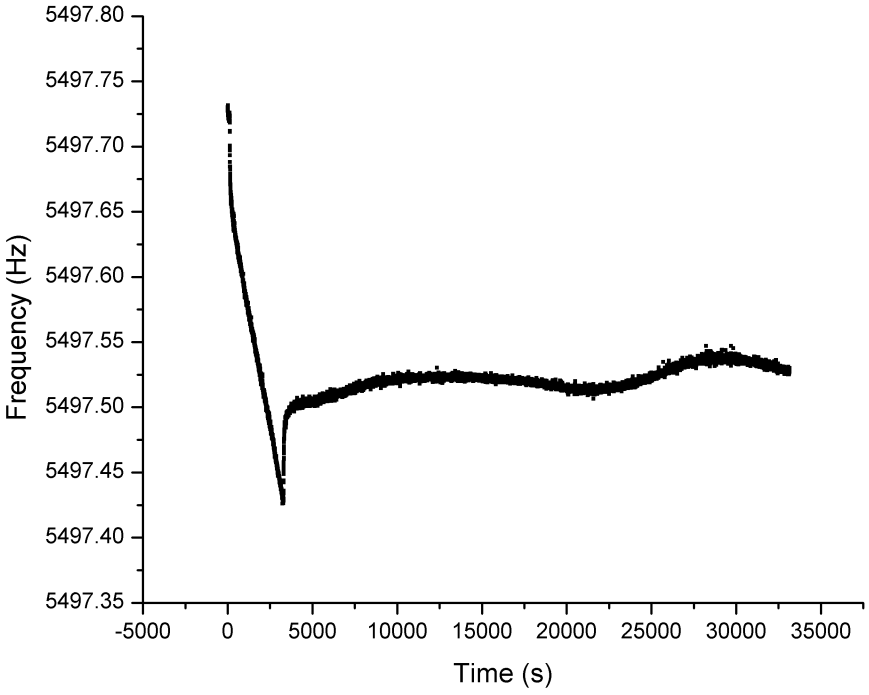

Figure 3.9: Bombardment run along with several hours of relaxation. Periodicity is slightly evident.

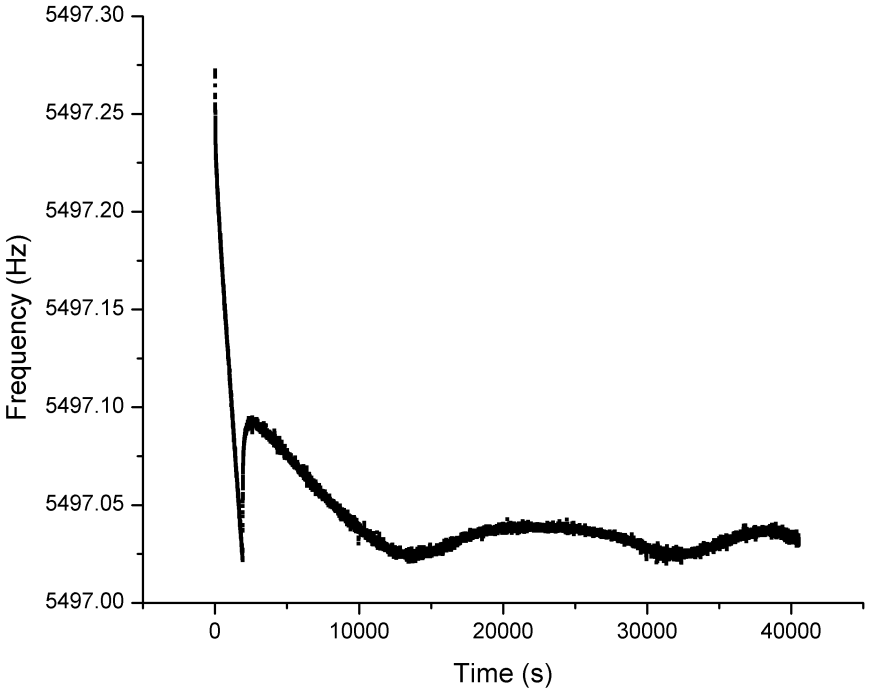

Figure 3.10: Bombardment run along with several hours of relaxation. Some periodicity with some type of initial drop in frequency

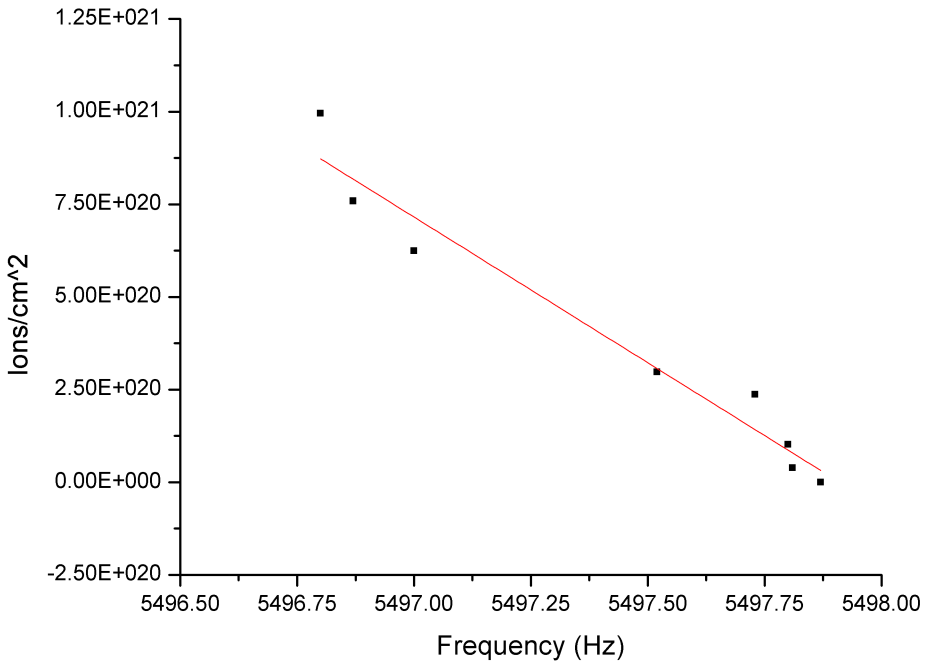

Figure 3.11: Change in resonant frequency by dose.

3.4 Relaxation and Non-Reversible Damage

After the beam is turned off the compressive stress relaxes very rapidly and the resonant frequency rises back to near the frequency observed in section one. This relaxation effect is likely tied to the DPO cooling and to diffusion processes inside the lattice [27]. Depending on the magnitude of the dose the DPO can take from hours to days for the frequency to equilibrate as observed through our bombardment runs. An example of this relaxation can be seen in Fig. 3.8, Fig. 3.9, and Fig. 3.10. There is some periodicity that can be seen from these data runs. This may be due to heat conduction down the manipulator from outside of the vacuum chamber. For example, additional bombardment

runs along with careful temperature control could identify or even control for this effect. While the resonant frequency of the DPO does relax back to near the initial frequency, as seen in Fig. 3.8, there is a slight overall change. This slight change could be attributed to damage near the surface of the neck from crystal amorphization. Ions that have cascaded through the lattice break up the crystal and the silicon can become amorphous. Amorphous silicon is less dense than the crystalline phase and also has a lower Young's modulus which in turn lowers the frequency of the resonance. Sputtered ions may also reduce the cross-sectional area of the neck thus reducing the total spring constant of the oscillator (see equation 3.7). A SRIM calculation of the sputter yield of Ar at 3 KeV is 1.04 atoms removed per ion. This obviously will reduce the size of the neck and lower the DPO's moment by a small ammount. However a lowering of the moment of the DPO would increase the frequency, an outcome not clearly observed. Therefore this final shifted frequency appears to be dominated by damage to the surface lattice while perhaps being slightly reduced by sputtered surface atoms. Overall the number of incident ions seems to lower the resonant frequency at a rate of $-7.86x10^{20} Hz/ions/cm^2$ with a standard error of $\pm 6.6x10^{19} Hz/ions/cm^2$ as seen in Fig. 3.11. The final frequency seemed more dependant on dose than on energy which may either correlate to lattice damage or sputtered atoms reducing the size of the neck thereby reducing the "spring constant" of the DPO. More runs would be required to sperate these two different processes.

3.5 Estimate of Shear Modulus Change

While the exact effect of Ar implantation on the shear modulus is near impossible, it is possible to approximate it. This approximation is based off of

a technique used by Tom Metcalf to find the shear modulus of noble gas thin films and more information about its origins can be found in his thesis [18]. This approximation is constructed around a ratio of frequencies to modulii,

$$\frac{\Delta f}{f} = \frac{3G_f(t_s^*)^2 t_f}{2G_s t_s^3} \tag{3.10}$$

where the t(s) are thicknesses. These thicknesses are illistrated in Fig. 3.12. The t(s) are thicknesses of a sputtered region (t_r), a damaged region (t_f), and an undamaged substrate (t_s^*). The initial thickness is t_s. G_s and G_f are the shear modulii of the substrate and damaged region respectively. As we know the frequencies and not the shear modulii we turn around the equation into

$$\frac{G_f}{G_s} = \frac{2\Delta f(t_s)^3}{3f(t_s^*)^2 t_f} \tag{3.11}$$

so the modulii are with respect to the known values. I solved for the ratio of change in shear modulus using data from all my runs used and SRIM calculations to find the ”approximate" thicknesses. My calcucated change over all of my runs was G_f/G_s = 0.2. Using values from literature for amorphous silicon and crystalline silicon the calulated change was G_f/G_s = 0.6 [28]. There are possibly several reasons why these values differ by an order of magnitude. One possible explanation could be due to ion channeling. Studies have shown that ions can channel down paths in an aligned crystal stucture [29]. It can be seen from equation 3.11 that if the damaged region (t_f) was thicker, our approximate value might be much closer to the accepted ratio of amorphous shear modulus to crystalline shear modulus. Another possiblility might be recrystalization of the lattice during relaxation, as described in the previous section, which might produce a shear

modulus much closer to that of crystaline silicon.

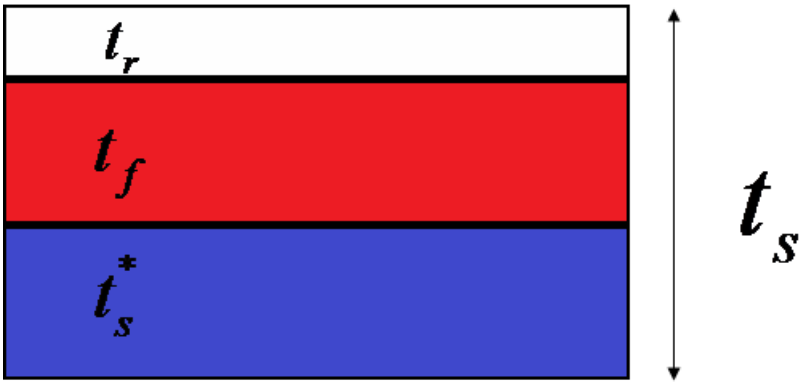

Figure 3.12: Three regions used in a shear modulus approximation. At the top t_r, is the thickness material removed by sputtering. In the middle t_f is the thickness of the region damaged by implantation. At the bottom, t_s^*, is the thickness of the undamaged DPO and in our case is much larger than the other two thicknesses. The whole substrate was initially t_s thick.

3.6 Summary

As DPOs are bombarded we observed five main regions of interest as seen in Fig. 3.1. Regions two and four, which show abrupt time-dependent resonant frequency shifts were discussed in terms of a compressive stress that increases the overall volume in the irradiated neck. However, this implantation related effect appears to saturate rapidly and a constant flux must be maintained to keep the reduction in modulii. Beyond the compressive stress, heating of the neck appears to become the dominant factor affecting the frequency. The heating causes a linear change in the frequency that can be related to a linear change in the Young's modulus. After the beam is turned off the frequency slowly returns to a value near the pre-irradiation frequency. However non-reversable damage caused by

the ion beam appears to lead to a final frequency that is consistently lower. This frequency reduction has a direct relationship with the total ion dose, and is likely tied to damage in the lattice and sputtering of the surface atoms.

Chapter 4

Conclusion

4.1 Summary

Because mechanical oscillators have resonant modes that are sensitive to their physical properties they are effective as both probes and sensors [10, 11, 12]. The main properties that control a mechanical oscillator are its moment and its Young's modulus. The moment is defined by the shape of the oscillator and its mass while the Young's modulus is based on the atomic binding and crystal structure. In this thesis I used double paddle oscillators (DPOs) to probe how ion beams can modify the crystal structure of silicon. I have described the construction of an apparatus for the excitation and measurement of a DPO's resonant frequency in ultra high vacuum for the purpose of measuring changes in their properties under ion irradiation. Results of ion irradiation runs were then discussed and some specific conclusions were drawn about the precision of DPOs as oscillators for mechanical spectroscopy.

4.2 Experimental Overview

The basic idea of the experiment was to irradiate an oscillating DPO in vacuum and monitoring how the resonant frequency changes. The electrical signal from an oscillating DPO is phase shifted and fed back into it as a driving force making it self resonating. The resonant frequency was then recorded for analysis. A mask was placed between the ion gun and the DPO so that only the neck can be irradiated as illustrated in Fig. 4.1. When the DPO is oscillating in the AS2 mode, the only mode used in this experiment, almost all of the energy during a cycle is stored in the neck. For this reason, mechanical changes made to the crystal lattice in the neck have a large impact on the resonant frequency of the DPO. Changes in internal friction of the bulk material in the neck occur during irradiation; however, the background electrical noise in our setup prevented us from deducing the impact ion irradiation has on a DPO's quality factor.

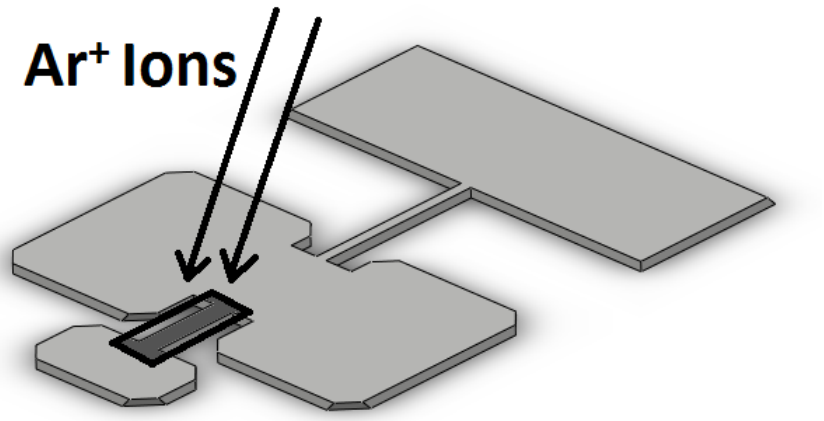

Figure 4.1: Example of the irradiated region on a DPO. The black rectangle is a representaion of the aperture on the mask.

4.3 Results

When the ion beam is turned on the resonant frequency suddenly drops, but after 20-30 sec the resonant fequency change becomes linear with time. During bombardment of a DPO the resonant frequency drops suddenly when the ion beam is turned on then changes linearly. When the beam is turned off the frequency jumps back up then slowly relaxes over several hours. An example set of data showing the frequency during a bombardment run is shown in Fig. 4.2. Regions two and four may be explained by a volume expansion in the regions where the ions are implanted while the linear region in between them is probably due to heating. Region five is where the DPO's resonant frequency relaxes to near its pre-bombardment frequency over several hours to days and the culprit is most likely slow diffusion processes. However, there is a slight shift downward in the post-bombardment steady state resonant frequency that seems to be linearly dependent on the total implanted dose and could be caused by non-reversible crystal lattice amorphization in the implanted region. As a whole, the DPO seems to work as a fairly precise tool for measuring damage in the crystal lattice, in real-time, during ion bombardment.

4.4 Future Work

The majority of the future work concerns problems in the experimental problems that were unsolved. The largest unsolved problem was the large amount of variation in the quality factor measurements. When measuring the quality factor, measurements that were taken moments apart would have large variations; the variations on the order of the values themselves. This led me to discard all of

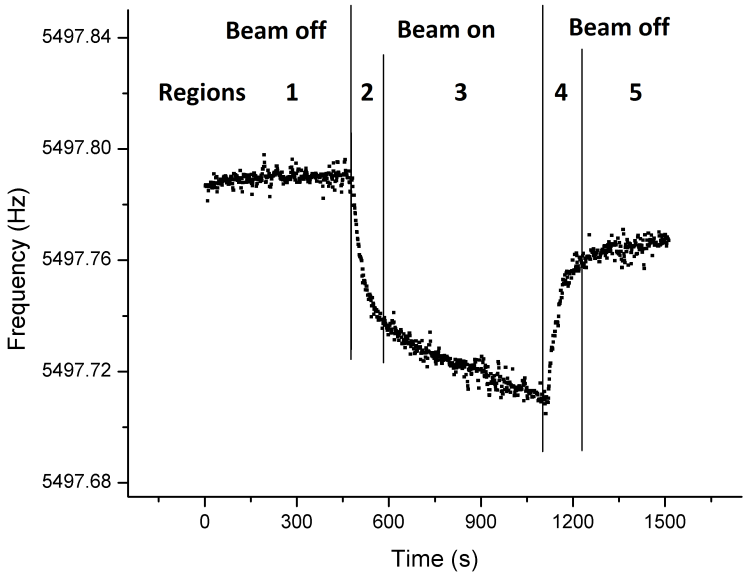

Figure 4.2: Regions of interest during an ion bombardment run.

the quality factor measurements. The primary reason for the variations, I believe, was amplification in the excitation system. The wiring and electrodes that we used had a large amount of electrical coupling that increased the return signal significantly. The lock-in amplifier (SRS-830) had to have its internal gain set by the user. So when then drive signal was cut, the return signal would almost disappear on the lock-in. This meant that we could only observe the decaying signal before it hit the lower limit for around 30 seconds. This low sample count, I believe, reduced the accuracy of the fits. For future experiments some significant work on decreasing this electrical coupling needs to occur. Special "Microdot" coaxial cables, the ones Tom Metcalf uses, could help to reduce much of this noise. Other designs of the electrodes could reduce this problem such as increasing the number of electrodes to 4. This design would utilize normal and inverted signals

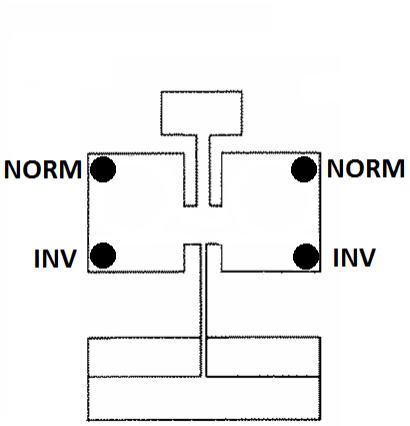

Figure 4.3: A possible solution to reduce coupling noise.

to front and back electrodes respectively as illustrated in Fig. 4.3. This would limit the resonant modes that would be excitable but would reduce much of the crosstalk in the wiring and at the electrodes. Also there are excitation methods that just use a single port thereby eleminating crosstalk entirely but require a completely different system [30]. Systems such as the one-port or the four-port method should be researched before another excitation system is created.

We believe that heating was the driving force in region three of bombardment runs (see section 3.3), however not much data backs this up. More could be learned about this by taking a broken DPO and mounting a thermocouple on the back of it then performing bombardments runs on it to observe the actual amount of heat produced by the impacting ions. Differential scanning calorimetery could then be performed on another piece of the same DPO to determine the thermal characteristics and thus allow for a thermal gradient map to be determined. Measures like these could find heating of the DPO as a function of ion irradiation by dose and energy.

When the DPO relaxes we think that it is caused by both thermal and

atomic diffusion. To further our understanding of how ion irradiation impacts resonating DPOs; runs should be performed both at low and high energies to determine how much of an effect diffusion has on the DPO during and after bombardment. If the DPO was cooled then bombarded at a much lower temperature, and the frequency did not climb after the beam was turned off then that would point toward diffusion as the mechanism for relaxation in the final region. A bombardment at higher temperatures, when diffusion is greater, would also prove or disprove this theory.

Once all the parameters controlling DPO oscillations are well understood, DPOs could become a valuable tool for analyzing material coatings under ion bombardment. It would most likely have applications for materials testing for spacecraft which often operate under ion bombardment from solar wind. Material coatings could be applied to the neck of the DPO which could then be irradiated to determine their impact on mechanical changes caused by such radiation.

Appendices

Appendix A Recording Data with GPIB

All the data was taken by a computer over GPIB. Because we did not have an available computer with a GPIB card I used a Prologix USB to GPIB converter. I used a program called EZGPIB to take the data. EZGPIB is essentially a Pascal compiler with a special set of libraries designed to work with the Prologix converter. The following code was used to take data during the bombardment runs. The program loops at a rate of one second in which it queries the frequency counter (SR620) and writes the new data on the next line of the text file. The name and location of the text file is defined at the beginning of the code. If the name of the file already exists it will overwrite the old text file. The program will run untill a key is pressed on the keyboard.

```
Program dpofreq;
{const counter = 16;     //Address of the SR620
filename = 'C:\users\dashiva\desktop\dpo\ion4\Ion4_1_4.Txt';
var answer1:string;
var freq:string;
procedure writefiledata;
begin;
  ezgpib_fileclearbuffer;
  ezgpib_fileaddtobuffer(answer1);
  ezgpib_filewrite(filename);
end;
begin;
if EZGPIB_FileExists(Filename)
then EZGPIB_FileDelete(Filename);
```

```
freq := 'MEAS?0';  //Command to read the SR620
  repeat
    EZGPIB_timeWaitformultipleof(1);
    EZGPIB_BusWriteData(counter,freq)
    EZGPIB_BusWaitForData(counter,answer1,3);
    writefiledata;
  until EZGPIB_KbdKeypressed;//Run untill keyboard is pressed.
end.
```

Taking the data to find the quality factor involves recording the amplitude of the oscillations at one second intervals from the lock-in. The following code is very similar to the one used above and differs only silightly. The data is recorded in a similar fashion and the program operates in much the same way. The only difference is that the SRS-830 lock-in is queried instead of the SR620. The lock-in needs to be in R θ mode for the program to record the correct information.

```
Program dpoQ;
const lockin = 8;
filename = 'C:\users\dashiva\desktop\dpo\ion5\Ion5_Q_start3.Txt';
var answer1:string;
var amp:string;
procedure writefiledata;
begin;
  ezgpib_fileclearbuffer;
  ezgpib_fileaddtobuffer(answer1);
  ezgpib_filewrite(filename);
end;
```

```
begin;
if EZGPIB_FileExists(Filename)
then EZGPIB_FileDelete(Filename);
amp := 'outr?1';
  repeat
    EZGPIB_timeWaitformultipleof(1);
    EZGPIB_BusWriteData(lockin,amp)
    EZGPIB_BusWaitForData(lockin,answer1,1);
    writefiledata;
    EZGPIB_ScreenWriteln(answer1);
  until EZGPIB_KbdKeypressed;
end.
```

When a new DPO is inserted into the chamber it must be scanned to find the relative locations of the resonance frequency of choice. The following code is used. It was also written to work with EZGPIB. The program scans the frequency source (DS335) between the variables xstart and xstop at a rate of 0.25 seconds stepping by the variable xstep. Within each step the amplitude and the phase are read from the SRS-830 lock-in. The SRS-830 needs to be in R θ mode for proper data to be read. The program stops of its own accord when the frequency reaches xstop. I would suggest maunally setting the DS335 to the start frequency to avoid a discontinuity at the onset of the program. The data is recorded in a similar manner to the previous two programs.

```
Program dpoacquisition;
const lockin = 8;  //srs-830 address
```

```
freqgen = 22;  //ds335 address
filename = 'C:\users\dashiva\desktop\dpo_stm_test20.Txt';
xstart = 5480;
xstop = 5500;
xstep = 0.5;
var answer1:string;
var answer2:string;
var current:double;
var amp:string;
var theta:string;
var freq:string;
procedure writefiledata;
begin;
  ezgpib_fileclearbuffer;
  ezgpib_fileaddtobuffer(current);
  ezgpib_fileaddtobuffer(answer1);
  ezgpib_fileaddtobuffer(answer2);
  ezgpib_filewrite(filename);
end;
begin;
if EZGPIB_FileExists(Filename) //Comment this out if you
then EZGPIB_FileDelete(Filename);
amp := 'outr?1';
theta := 'outr?2';
current := xstart;
  repeat
```

```
  freq:= 'freq';
    //EZGPIB_timeWaitformultipleof(3);
    EZGPIB_ConvertAddToString(freq,current)
    EZGPIB_BusWriteData(freqgen,freq);

    EZGPIB_BusWriteData(lockin,amp)
    EZGPIB_BusWaitForData(lockin,answer1,1);

    EZGPIB_BusWriteData(lockin, theta)
    EZGPIB_BusWaitForData(lockin,answer2,1)

    Answer1:=EZGPIB_ConvertStriptoNumber(Answer1);
    EZGPIB_ScreenWriteln(current);
    EZGPIB_ScreenWriteln(Answer1);
    EZGPIB_ScreenWriteln(Answer2);
    writefiledata;
    current := current + xstep;
  until current >= xstop;
end.
```

Appendix B Current to Voltage Converter

The current to voltage converter was used as the first amplification performed on the signal from one of the manipulator electrodes. One of the paddles of the DPO is situated above the sense electrode and the two form a capacitor that is utilized to detect paddle movement. The capacitor equation

$$C = \frac{Q}{V} \tag{1}$$

is well known and describes the relationship between capacitance (C), charge (Q), and voltage (V). A parallel plate capacitor behaves according to

$$C = \frac{\epsilon A}{r} \tag{2}$$

where ϵ is the dielectric constant, A is the area, and r is the separation between the plates. Because the voltage across this ”capacitor" is constant (see section 2.2) the charge (Q) must change in time as the plate separation (r) changes in time. Combining equations B.1 and B.2 while using a time dependant r, gives us

$$-\left(\frac{1}{r^2}\right)\frac{dr}{dt} = \frac{1}{\epsilon A V}\frac{dQ}{dt} \tag{3}$$

where dQ/dt is by definition the current. From this it becomes clear that as the DPO oscillates it produces a time varying current change. Because the lock-in amplifier input has a high input impedance the signal must be converted from a current to a voltage before it can be utilized. Fig. 4-a. shows a schematic of the current to voltage amplifier that we used. It was designed for an amplification of 10^9 Volts per Amp. We did not have access to ultra-low tolerance resistors,

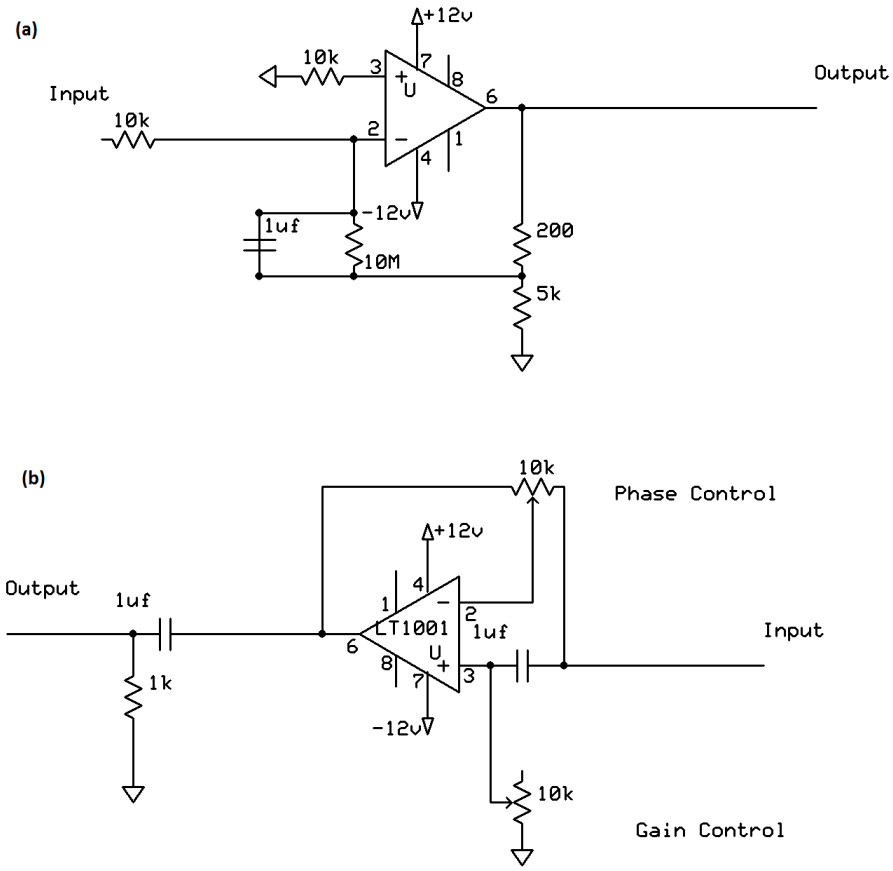

Figure 4: Schematic of the Current Amplifier (a) on top and of the Phase Shifter (b) below.

when constructing the amplifier, so the gain is probably slightly different. For this reason the exact displacement of the DPO is unknown as the amplifier was never fully characterized. This circuit design is based on one from a well known circuit design book [22].

Appendix C Phase Shifter

It can be observed from equation B.3 that the current produced by DPO oscillations does not correspond directly to the actual position of the DPO. Also, as the signal goes goes through the electronics it becomes shifted slightly by signal filters. For these reasons the drive signal must be phase shifted so that the DPO excites itself properly. To perform the phase shifting several techniques were initially deployed with varying levels of success. The technique that was finally settled upon utilized an all-pass filter to phase shift the signal. The all-pass filter design was taken from an electronics handbook and incorporated potentiometers to allow manual adjustment of both gain and phase [22]. The final design can be seen in Fig. 4-b. A simple high-pass filter was later added to the output to try to prevent the DPO from occasionally switching to the low frequency CL1 mode and can be seen on the left side of Fig 4-b next to the output.

Bibliography

[1] K. Dahmen, M. Giesen, J. Ikonomov, K. Starbova, and H. Ibach, "Steady-state surface stress induced in noble gas sputtering," Thin Solid Films **428**, 6–10 (2003)

[2] M. Moore, N. Kalyanasundaram, and et. al., "Structural and sputtering effects of medium energy ion bombardment of silicon," Nuclear Instruments and Methods in Physics Research B **241-255**, 241–255 (2004)

[3] C. A. Davis, "A simple model for the formation of compressive stress in thin films by ion bombardment," Thin Solid Films **226**, 30–34 (1993)

[4] S. Huang, B. Li, and X. Zhang, "Elimination of stress-induced curvature in microcantilever infrared focal plane arrays," Sensors and Actuators **130-131**, 331–339 (2006)

[5] A.J. Perry, D.E. Geist, K. Narasimhan, and J.R. Treglia, "On the state of stress in the surface of ground cemented carbide before and after metal ion implantation," Surface and Coatings **86-87**, 364–371 (1996)

[6] M. Legodi, S. Auret, and et al., "Schottky barrier modifcation and electrical characterization of low energy he-ion bombardment induced defects in n- and p-type gaas," Nuclear Instruments and Methods in Physics Research B **148**, 441–445 (1999)

[7] M. Tomura, C. Huang, S. Samukawa, and et al, "Mechanism of mechanical deterioration in silicon microcantilever induced by plasma process," in *IEEE Sensor Conference* (2010)

[8] W.L. Chan, E. Chason, and C. Iamsumang, "Surface stress induced in cu foils during and after low energy ion bombardment," Nuclear Instruments and Methods in Physics Research B **257**, 428–432 (2007)

[9] K. Chiu, Z. Barber, and R. Somekh, "The control of film stress using ionised magnetron sputter deposition," Thin Solid Films. **343-344**, 39–41 (1999)

[10] A. Markidou, W.Y. Shih, and W.H. Shih, "Soft-materials elastic and shear moduli measurement using piezoelectric cantilevers," Review of Scientific Instruments **76** (2005)

[11] S. Galliou and M. Mourey, "Electro-thermal simulation of an ultra stable quartz oscillator," International Simulation of Thermal Sciences **41**, 171–181 (2002)

[12] N. Rong, Z. Xiao-Bing, and et. al., "Piezoelectric quarz crystal sensor array with optimized oscillator circuit for analysis of organic vapors mixtures," Sensors and Actuators B **88**, 198–204 (2003)

[13] F. Walls and J. Gangepain, "Enviromental sensitivties of quartz oscillators," IEEE Transactions on Ultrasonics, Ferroelectrics, and Frequency Control **30** (1992)

[14] L. Rodriguez-Pardo, J. Farina, and et al., "Resolution in quarz crystal oscillator circuits for high sensitivity microbalance sensors in damping media," Sensors and Actuators B. **104**, 318–324 (2004)

[15] P. Rosner, K. Samwer, and R.O. Pohl, "Use of a double-paddle oscillator for the study of metallic films at high temperatures," Review of Scientific Instruments **74**, 3395 (2003)

[16] L. Christoph, Spiel, and R. O. Pohl, "Normal modes of a si 100ÂĚ double-paddle oscillator," Review of Scientific Instruments **72**, 1481–1492 (2001)

[17] R.N. K!eiman, G.K. Kaminsky, R. Pindak J.D. Reppy, and D.J. Bishop, "Single-crystal silicon high-q torsional oscillators," Review of Scientific Instruments **56**, 2088 (1985)

[18] T. H. Metcalf, *Elastic Properties, Annealing, and Vapor Pressure of Neon and Argon Films*, Ph.D. thesis, Cornell University (2002)

[19] T.H. Metcalf, Xiao Liu, B.H. Houston, J.E. Butler, and T. Feygelson, "Role of filmâĂŞsubstrate interface in the internal friction of nanocrystalline diamond films," Journal of Mechanical Science and Technology A **442**, 332–335 (2006)

[20] T. Burkert, J. Classen, C. Enss, and S. Hunklinges, "Internal friction of vitreous silica measured with a double paddle oscillator," Physica B **284-288**, 1133–1134 (2000)

[21] U. Gysin and P. Rast et al., "Temperature dependace of the force sensitivity of silicon cantilevers," Physical Review B **49**, 1–6 (2004)

[22] Hill W. Horwitz P., *The Art of Electronics*, 2nd ed. (Cambridge University Press, 1980, 1989)

[23] N. Kalyanasundaram, M.C. Moore, J.B. Freundb, and H.T. Johnson, "Stress evolution due to medium-energy ion bombardment of silicon," Acta Materialia **54**, 483–491 (2006)

[24] Poole C. Safko. Goldstein, H., *Classical Mechanics*, 11th ed. (Pearson Education, Inc, 2002)

[25] J. Wachtman, W. Tefft, D. Lam, and C. Apstein, "Exponential temperature dependence of young's modulus for several oxides," Physical Review Letters **122** (1963)

[26] M. Nandanpawar and S. Rajagopalan, "Wachtman's equation and temperature dependence of bulk moduli in solids," Applied Physics **49** (1978)

[27] R. Nowak, Y. Miyagawa, and et al., "Post-deposition reduction of internal stress in thin films: The case of hfn coatings bombarded with au ions," Material Letters **33**, 31–36 (1997)

[28] M.A. Hopcroft, W.D. Nix, and T.W. Kenny, "What is the young's modulus of silicon?." Journal of Microeletromechanical Systems **19**, 229–238 (2010)

[29] E. Morvan, P. Godignon, and et al., "Montecarlo simulation of ion implantation into sic-6h single crystal including channeling effect," Materials Science and Engineering: B **218-222**, 218–222 (1997)

[30] J. Bienstman, A.C. Harris, and et. al., "An oscillator circuit for electrostatically driven silicon based one-port resonantor," Sensors and Actuators **52**, 179–186 (1996)